ON THE PERFORMANCE OF TILTING PAD BEARINGS: A NOVEL MODEL FOR LUBRICANT MIXING AT OIL FEED PORTS WITH IMPROVED ESTIMATION OF PADS' INLET TEMPERATURE AND ITS VALIDATION AGAINST EXPERIMENTAL DATA

Luis San Andrés
Mast-Childs Chair Professor
Mechanical Engineering Department
Texas A&M University
College Station, TX, USA
Lsanandres@tamu.edu

Behzad Abdollahi
Mechanical Engineer
LobePro Rotary Pumps
Brunswick, GA, USA
Behzad.Abdollahi90@gmail.com

Luis San Andrés performs research in fluid film lubrication and rotor dynamics, having produced significant advances in hydrostatic bearings for primary power cryogenic turbo pumps, squeeze film dampers for aircraft jet engines, and gas foil bearings for oil-free micro turbomachinery. Luis is a Fellow of ASME and STLE, and a member of the Industrial Advisory Committees for the Texas A&M Turbomachinery Symposia. In 2016, Dr. San Andrés chaired the I Asia Turbomachinery & Pump Symposium in Singapore. Dr. San Andrés has educated dozens of graduate students serving the profession with distinction. Dr. San Andrés earned a MS in ME from the University of Pittsburgh and a PhD in ME from Texas A&M University. Luis has published over 160 journal papers, several recognized as best in various international conferences. His URL site http://rotorlab.tamu.edu offers free resources on lubrication, dynamics and vibrations for students and practicing engineers.

Behzad Abdollahi* received his B.S. degree in Aerospace Engineering from Sharif University of Technology in Tehran, Iran. He discovered his passion for turbomachinery and rotating equipment and decided to further his education with an M.S. degree at Texas A&M University. He worked as a Graduate Research Assistant at the Turbomachinery Laboratory under Dr. Luis San Andrés. His research primarily focused on computational analysis of fluid film bearings and rotordynamics. Behzad is a Mechanical Engineer at LobePro Rotary Pumps working on research and development projects.

ABSTRACT

Energy efficient operation of fluid film bearings demands savings in delivery flow while also managing to reduce fluid film and pad temperatures. To achieve this goal, tilting pad journal bearings (TPJBs) implement a variety of oil feed arrangements (LEG, spray bars, etc.), use pads with highly conductive material and engineered back surface, and also end seals to keep (churning) lubricant within the bearing housing. Often, to evidence the savings, operators supply bearings with a fraction of the flow predicted by an analysis, independently of the system operating speed and likely (dynamic) load condition.

The lecture briefs on an analysis of TPJBs that includes pivot flexibility and pad surface deformation due to hydrodynamic film pressure and pad crowning due to thermal effects. The work introduces a novel model for the mixing of flow and thermal energy at a lubricant feed port, which sets the temperature of the lubricant entering a pad leading edge. Precise estimation of this temperature (and inlet oil viscosity) and the flow rate entering a pad largely determine the temperature rise along the pad lubricated surface as well as the shear drag power loss, and ultimately the bearing load capacity.

Over decades, conventional modeling of TPJBs implements a hot oil carry coefficient to estimate thermal mixing at a feed groove. This model requires an empirical constant that is a function of the operating conditions (speed and load) and is apparently the same for all pads in a bearing. The present thermal mixing model delivers improved temperature predictions in conditions that limit the conventional model. An important addition is the ability to impose the actual lubricant supply flow, specifically when the bearing is

---

* Work conducted as a graduate research assistant at Texas A&M Turbomachinery Laboratory.
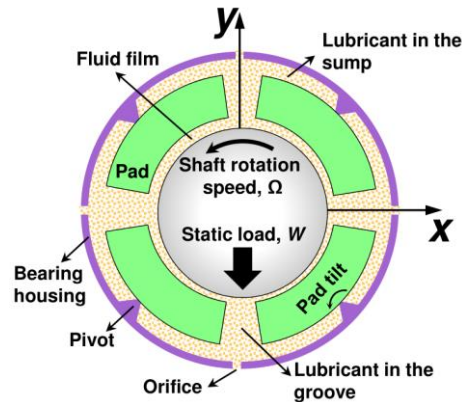
Figure 1: Schematic view of a 4-pad load between pad (LOP) tilting pad journal bearing components and coordinate system.

operating in either an over-flooded or a reduced flow condition. In addition, the flow balance in the new model accounts for the groove side leakage flow (discharging out of the bearing) and the churning (recirculating) oil in a groove or feed port. An empirical groove efficiency parameter regulates the temperature of the above-mentioned flows to represent conventional and direct (LEG, spray bars) lubricant feeding arrangements as well as end-sealed (flooded) or evacuated bearing configurations.

Predicted static and dynamic performance for two TPJBs are compared against two sets of published test data in Refs. [1-5]. One is a large 5-pad bearing (500 mm ID) with end seals and supplied with a flowrate as low as 50% of the nominal (predicted) condition. The rotor speed is 3 kRPM (79 m/s surface speed) and the maximum specific load equals 25 bar. The other bearing is a 4-pad (102 mm ID) operating with a fixed flow rate, invariant as the speed increases to 16 kRPM (85 m/s) with an applied load increasing from 7 bar to 29 bar. Comparisons with the first bearing include the film thickness, pressure and temperature fields around the bearing circumference, as well as journal static eccentricity and synchronous speed reduced force coefficients. The second bearing incorporates a variety of oil feed arrangements and offers dynamic force coefficients over a range of excitation frequencies. Bearing performance predictions using either the novel model or the conventional thermal mixing model, when compared against the test data, demonstrate the improvement.

The lecture concludes delivering recommendations for the feed port efficiency parameter for various types of oil supply configurations. This parameter does not change with the bearing operation conditions. Thus, bearing designers have a new tool that allows the early specification of flow rate as an input parameter, not a consequence of analysis nor a constraint during actual operation.

INTRODUCTION

A tilting pad journal bearing (TPJB) is a type of fluid-film bearing supporting rotating machinery. TPJBs are selected due to their lower shear power losses and minimal destabilizing forces when compared to a rigid surface bearing. A TPJB, as shown in Figure 1, consists of usually three to six pads, each supported by a pivot. There is a thin lubricant film between the pads and the spinning journal. During operation, each pad tilts about its pivot and forms a convergent wedge between the pad inner surface and the shaft. The journal surface drags the viscous fluid into the wedge to generate a hydrodynamic pressure field that enables the bearing to carry a load (W).

Figure 2(a) shows a conventional (single orifice[1]) feed groove in a TPJB. This region is comprised of an orifice supplying cold (fresh) lubricant at supply temperature (T_{sup}) into the groove, an upstream pad discharging warm lubricant into the groove along with a layer of hot oil (at temperature T_{TE}) attached to the journal surface, and a downstream pad that demands a certain amount of lubricant to fill its clearance. The flow within the groove is highly recirculating (churning).

Mixing of hot and cold flows along with thermal energy exchanges in the lubricant feed groove region set both the temperature and flow rate of the fluid entering the leading edge of a downstream pad [6]. The flow rate and temperature of the fluid at a pad leading edge largely determine the film temperature rise along the lubricated pad surface and the temperature field within the pad, both of which ultimately govern the pad and journal thermally induced deformations.

---

[1] Modern high performance TPJBs employ direct lubrication methods such as spray bars (with blockers) and leading edge grooves.
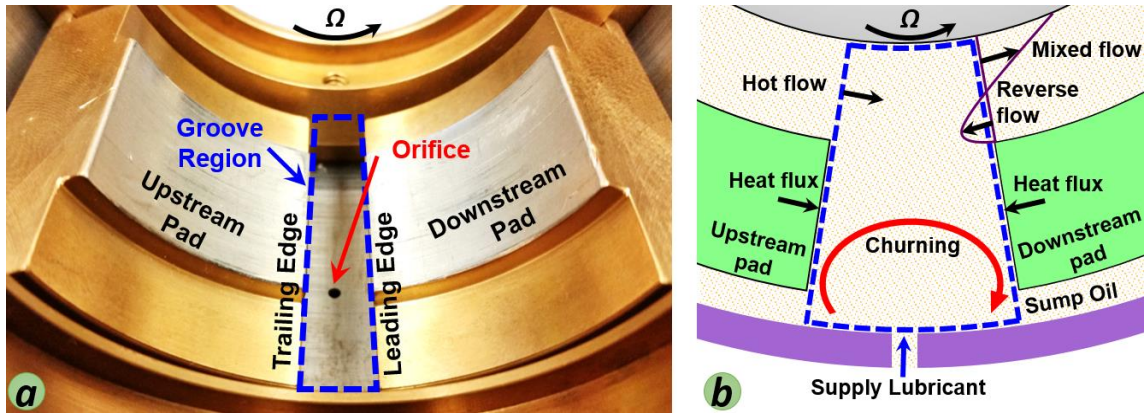
Figure 2: (a) A lubricant feed groove region bounded by adjacent pads in a TPJB with a single orifice; (b) Heat fluxes and lubricant flows across the boundaries of a feed groove region.

In spite of the intricate nature of the flows in the feed groove region, various authors (Refs. [7-9]) have developed simple though still physically sound models for the fluid mixing in this region. Bulk or lumped parameter thermal mixing models (adopted from Ref. [7]), apply the conservation of mass and thermal energy in the groove region through a thermal mixing coefficient or hot oil carry over factor ($0 < \lambda < 1$). The parameter λ represents the fraction of flow leaving an upstream trailing edge (Q_{TE}) at temperature T_{TE}. This flow mixes with the supply lubricant flow (Q_{sup}) injected in the groove at (cold) temperature T_{sup}. Entering the downstream pad is a flow with magnitude (Q_{LE}) at temperature T_{LE}. A lumped parameter mass flow balance and a thermal energy flow balance determine the leading edge temperature (T_{LE}) and flow rate (Q_{LE}) as

$$
\begin{aligned}
Q_{sup} &= Q_{LE} - \left(\lambda Q_{TE} \right) \\
T_{LE} Q_{LE} &= Q_{sup} T_{sup} + \left(\lambda Q_{TE} \right) T_{LE}
\end{aligned}
\tag{1}
$$

This simple concept, adapted by virtually all prediction tools, is not accurate for bearings operating under certain extreme conditions, see Ref. [10]. Some recent works [1, 2, 10-12] report models for the fluid mixing in the feed groove region that diminish the influence of empirical coefficients. The following lists several physical phenomena within the groove region that are not accounted for by a simple (conventional) thermal mixing flow model.

Figure 2(b) depicts the heat fluxes and fluid flows across the boundaries for a single orifice lubricant feed, i.e. a conventional or traditional oil supply arrangement. The cold supply flow mixes with the churning oil in the groove region before reaching the (upstream) hot oil layer attached to the rotating shaft. Meanwhile, the adjacent pads exchange heat with the oil in the groove via the bounding side walls. The fluid film entering a pad adds the shear driven flow (dragged by the spinning journal) to the pressure driven (reverse) flow. As the applied load increases the pressure driven flow becomes dominant causing a portion of the lubricant at the pad leading edge to flow in a reverse direction and to re-enter the groove. Finally, a portion of the flow exits the groove region axially (side leakage) depending on whether the bearing has end seals (flooded) or not (evacuated).

Figure 3 shows a load-between-pad (LBP) four pad TPJB operating under a heavy specific load ($W/(LD) > 2.1$ MPa). A high journal eccentricity in the load direction creates a very thin film in the bottom pads while it unloads the upper ones, thus leaving a large gap between the unloaded pads (3, 4) and the shaft. The groove in between pads 4 and 1 receives a large flow (Q_{TE}) from unloaded pad #4, while discharging only a much smaller flow (Q_{LE}) to be carried into the heavily loaded pad #1. The conventional thermal mixing model, Eq. (1), assumes that the supply flow (Q_{sup}) always enters the groove; however in this condition, since (λQ_{TE}) > Q_{LE} the model sets the supply flow rate (Q_{sup}) to zero. Ettles [9] defines boundaries for a ratio of upstream flow to downstream flow that prevents a negative supply flow. In this situation Suh and Palazzolo [13] also modify the model in Eq. (1) to bypass the flow rate balance.
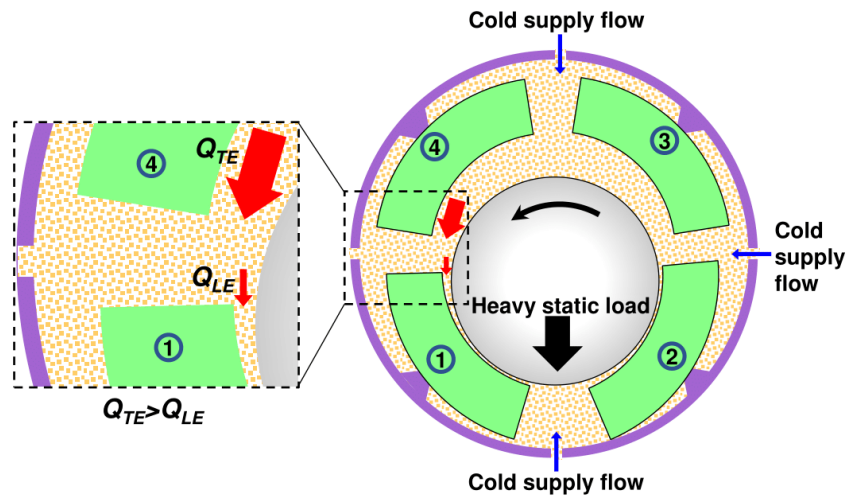
Figure 3: A heavily loaded TPJB operating with a large shaft eccentricity (small film thickness).

Brito et al. [10] observe experimentally that in a two-groove plain journal bearing hot oil flows out through one of the feed orifices (hot oil reflux) when the groove region is in the vicinity of the load direction. However, a similar phenomenon (hot oil reflux) is not likely in TPJBs.

TPJBs with direct lubrication often operate with no end seals or wide open seals (evacuated housing) [14], and the excess upstream oil leaves the groove region axially (side leakage) [15]. For either a flooded or an evacuated bearing configuration, including the side leakage flow in the groove lubricant mixing model improves the temperature prediction (as in Ref. [12]).

THE WORK BEFORE

The majority of methods that evaluate the film temperature at the leading edge of a pad (downstream of a groove) adopt an approximate lumped parameter balance of both flow and thermal energy. In spite of complexity of the flow in a lubricant feed groove region, simplified models arose for arc journal bearings [6] and thrust bearings [16], and later extended to TPJBs [9]. In addition, modern high performance TPJBs use direct lubrication methods that further make a difference between TPJB feed grooves from plain journal bearings feed grooves. Nevertheless, the various approaches to modeling the fluid mixing at a feeding groove in plain journal bearings helps with understanding this phenomenon in TPJBs.

In 1983, Mitsu et al. [7] investigate experimentally the effect of oil flow rate on fluid mixing at a feed groove in a plain journal bearing and introduce the mixing model in Eq. (1). The authors vary the supply pressure between 20 kPa and 180 kPa (to change to supply flow rate) for an operation with a constant shaft speed of 1750 RPM ($\Omega R_s = 9$ m/s) and a specific load of 0.5 MPa. Mitsu et al. introduce an empirical coefficient (λ) for the mixing of the lubricant flow with the supply flow prior to reaching the pad inlet. The measurements show that λ is inversely proportional to the supply flow rate and it lessens for an over-flooded condition ($\lambda \sim 0.3$). The authors conclude that a λ between 0.4 and 0.8 provides film temperature predictions that are closely aligned with the test data among various flow rates.

In 1986, Heshmat and Pinkus [8] define a function for the thermal mixing coefficient (λ) using the measured flow and temperature magnitudes in the feed groove of a plain journal bearing. The authors use a transparent bushing to observe the groove flow with a journal diameter of 138.1 mm, operating with a shaft speed of 1800 RPM ($\Omega R_s = 14$ m/s) and under a specific load of 690 kPa. Most of the flow in the oil groove is highly recirculating (churning) and has little effect on the fluid flow (and therefore heat flow) that enters the groove from the upstream pad or discharges to the downstream pad. The empirically estimated mixing coefficient (λ) is a function of surface speed and oil supply temperature, and not dependent on the type of oil or applied load. λ in Ref. [8] applies to a single pad and is adequate within the limited test range of oil supply temperature and journal surface speeds.

In 2012, He et al. [14] investigate the applicability of the model in Ref. [7], Eq. (1), to direct lubrication bearings in a thermo-hydrodynamic (TEHD) analysis. In industrial practice the coefficient (λ) is set as, $0.7 < \lambda < 1$ for conventional flooded bearings and $0.3 < \lambda < 0.7$ for directly lubricated bearings and evacuated bearings. The authors set a lower limit for a pad leading edge temperature

4

predicted from Eq. (1), and define a cool oil insertion model. Here, Q_{sup} is known, and without resort to a mixing coefficient, the trailing edge flow (Q_{TE}) equals (Q_{LE}- Q_{sup}), and

$$T_{LE}\,Q_{LE} = Q_{sup}\,T_{sup} + \left(Q_{LE} - Q_{sup}\right)T_{TE} \tag{2}$$

Eq. (2) represents a physical situation where all the available supply oil cools the minimum amount of hot oil in the most efficient way. He at al. [14] then compare TEHD predictions to test data for three direct lubrication bearings (spray bar and leading edge groove). The test bearings have a common diameter of 0.1016 m, operate with a shaft speed ranging from 4 kRPM to 16 kRPM (ΩR_s = 85 m/s), and under a specific load between 0.35 MPa and 3.1 MPa. For the largest load, predictions are less consistent with test data, within 10°C maximum difference; shaft speed having little effect on the discrepancy. The thermal mixing coefficient (λ) decreases with an increase in shaft speed. The predicted temperature for the first unloaded pad, downstream of loaded pads, is substantially higher than the measurement which casts doubt on the assumption of an evenly distributed supply oil into each groove, Q_{sup}/N_{pads}.

In a similar way, Suh and Palazzolo [13] in 2015 modify Eq. (1) and use a mixing coefficient (λ=0.8) when the upstream flow is larger than a portion of the (required) downstream flow. This is to prevent a zero or negative supply flow. In this case, the temperature at the leading edge is a weighted average of the temperature at the pad trailing edge and the temperature of the (cold) supplied lubricant,

$$T_{LE} = \lambda T_{TE} + (1-\lambda)T_{sup} \quad \text{when} \quad \left(\lambda Q_{LE}\right) < Q_{TE} \tag{3}$$

DESCRIPTION OF A NOVEL THERMAL MIXING MODEL

San Andrés and Tao [17] state an extended Reynolds equation governing the generation of the pressure field in a TPJB, accounting for temporal fluid inertia where the lubricant viscosity (μ) is a function of the film temperature.

The film thickness is a function of circumferential and axial coordinates. The elastic deformation of each pad inner surface modifies the film thickness along the radial direction and includes both thermally induced and pressure induced deformations. Ref. [18] implements a steady-state bulk flow energy transport equation for a steady state condition and an incompressible fluid. Viscous dissipation generates heat that disposes through convection and diffusion in the fluid film. The energy transport equation in the present model averages the fluid temperature across the film. The simplification offers a good balance between implementation complexity, quality of results, and calculation time [19].

About the Lubricant Mixing at a Feed Groove [20]

A major drawback of the conventional hot oil carry over model , Eq. (1), is that it predicts a supply flow only based on the upstream flow (Q_{TE}^{i-1}) and downstream (Q_{LE}^{i}) flow adjacent to a groove [7, 21]. Therefore, unless the predicted flow rates are close to actual ones, the conventional model gives an inaccurate leading edge film temperature (T_{LE}).

As stated earlier, He et al. [14, 22] assume each groove collects an identical fraction of the total flow supplied, namely

$$Q_{sup}^{i} = \frac{Q_{sup}^{total}}{n} \tag{4}$$

Ref. [22] clarifies that Eq. (4) does not always satisfy mass flow continuity condition in a feed groove. For operation with a high load (large journal eccentricity), as shown in Figure 4, the journal operates near the groove between pads 4 and 1. Here, the inlet film thickness of pad 1 reduces. In this situation, the authors [22] suggest that this groove acts as a flow restrictor, and receives less fresh lubricant due to a fluid pressure rise within the groove. The authors note that if a particular groove receives an excessive supply of oil, a fraction of it immediately displaces outwards as side leakage.

Figure 4 shows an idealized representation of the total supplied flow (Q_{sup}^{total}) dividing into separate streams (Q_{sup}^{i}). A deep outer groove on the bearing housing OD (plenum) contains the fresh lubricant at the supply temperature and feeds each orifice based on the
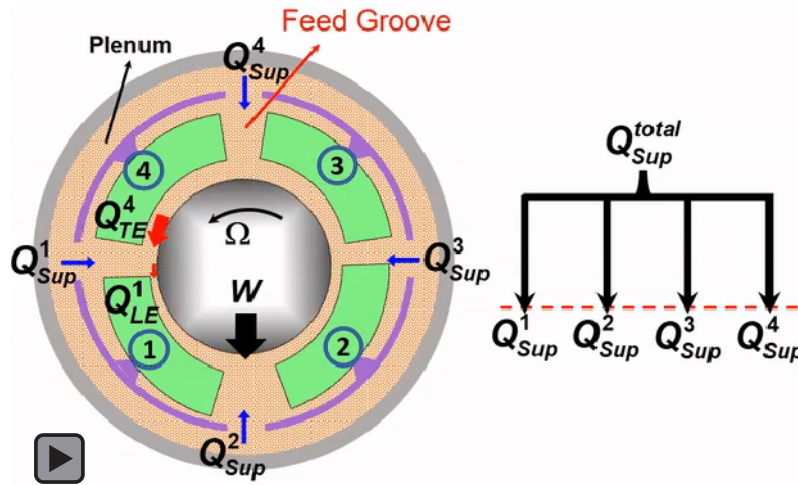
Figure 4: Left: schematic view of a heavily loaded TPJB operating at a large journal eccentricity. Right: a hydraulic network that allocates the supply flow into each feed groove.

groove local pressure on the other side of the hole. Due to the complexity of the flow in the groove region, determining a local pressure for the groove is not practical. Instead, the current model extends Eq. (4) to account for excessive flow demand or a restriction of flow from each groove.

Thin film lubrication theory defines the fluid circumferential velocity as a superposition of a shear driven flow dragged by the motion of the shaft (Couette flow) and a pressure driven flow (Poiseuille flow) [23]. The axial flow only comprises of a pressure driven flow. The circumferential flow at either a pad leading edge (θ_{LE}) or a pad trailing edge (θ_{TE}) equals

$$Q\big|_{\theta_{LE},\theta_{TE}} = Q_{shear} + Q_{pressure} \tag{5}$$

Figure 5 shows the fluid velocity profiles at the leading and trailing edges of a bearing pad. The integration of the velocity field across the gap produces the flow rate. The two top graphs (A & B) show the superposition of shear flow and the (retarding) pressure flow since $\partial P/\partial\theta > 0$ at θ_{LE}. The bottom graph (C) shows flow exiting a pad with $\partial P/\partial\theta < 0$ at θ_{TE}; here both the shear and pressure induced flows are in the same direction, $Q_{shear} > 0$ and $Q_{pressure} > 0$. In (A), the pressure gradient is small since the pad is likely unloaded, the fluid velocity profile is lesser than for the pure shear condition; and to fill the gap, the leading edge demands a large flow. As the pad becomes loaded, see (B), the film pressure increases and forces the lubricant in an opposite direction to the shaft surface speed, $Q_{shear} > 0$ and $Q_{pressure} < 0$. This effect significantly reduces the net flow rate $Q\big|_{\theta_{LE}}$. Most importantly, the top layer attached to the rotor surface carries (mainly) hot lubricant leaving through the trailing edge of the upstream pad.

The first step to quantify the restriction or demand of each groove for fresh (cold) lubricant, introduces a groove demand (C_i) parameter that accounts for the following:[2]

- At a pad leading edge, the shear driven (forward) flow (proportional to film thickness) increases the *demand* for (cold) supply lubricant. The pads with a large leading edge film thickness, as is the case for unloaded pads #3 and #4 (see Figure 4), receive a large flow at their inlet (leading edge). On the other hand, a large hydrodynamic pressure gradient (on loaded pads #1 and #2) may cause a significant flow in the reverse direction that curtails the flow demand.
- At a pad trailing edge, the pressure driven flow adds to the shear flow, pushing the flow in the same direction as the shaft surface motion. A large flow leaving from an upstream pad (Q_{TE}^{i-1}) may provide an excess amount of flow to fill in the gap of the downstream pad leading edge, and this reduces the demand for additional supply flow. The leading edge flow of pads #1 and #2 are about the same (see Figure 4), but pad #1 receives a large flow from upstream (usually hot), reducing its demand for supply oil. Similarly,

---

[2] Note the assumption is valid if all the pads are fully wetted (flooded) and able to maintain a full film throughout every pad.

the leading edge flow of pads #3 and #4 are about the same, but pad #3 receives a very small flow from the upstream which aggravates its need for more supply oil.
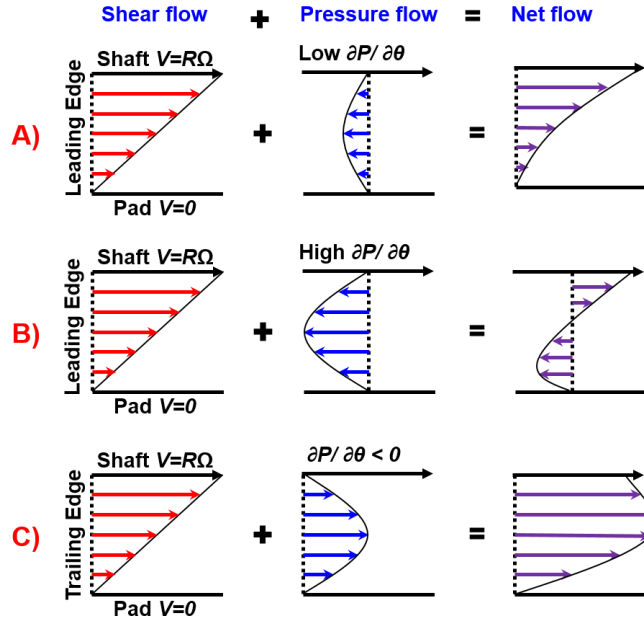

Figure 5: Illustrations of the film velocity profile entering a pad through its leading edge (A &B) and leaving a pad through its trailing edge (C).

Recall that the ith groove faces the trailing edge of an upstream pad $(i-1)$ and the leading edge of downstream pad (i). The demand parameter (C_i) for the ith groove divides the shear flow rate (Q_{shear}^i) entering i^{th} pad to the total flow that blocks the fresh supply of oil. The latter (blocking) flow adds the flow rate leaving the $(i-1)^{th}$ pad at its trailing edge (Q_{TE}^{i-1}) to the pressure driven flow exiting (in reverse) the leading edge of the ith pad $(-Q_{pressure}^i)$. The demand parameter is

$$C_i = \frac{Q_{shear}^i}{\left(-Q_{pressure}^i + Q_{TE}^{i-1}\right)}\bigg|_{i=1,\cdots,n} \tag{6}$$

$C_i = 1$ if both downstream pad and upstream pad flows are equal; that is the case of a centered journal (no load). $C_i < 1$ in the ith groove that restricts the supplied flow; whereas $C_i > 1$ for the ith groove that demands extra lubricant. The second step adds $C_i\big|_{i=1,\cdots,n}$ to produce a total demand parameter (C_{total}). The available total or global supply flow (Q_{total}) meets the total demand by the bearing.

$$C_{total} = \sum_{i=1}^{n} C_i \tag{7}$$

As the final step, a groove receives a portion of the total supply flow based on its demand (C_i) relative to the total demand (C_{total}). Here the grooves with a larger demand receive a greater portion of the supply flow.

Let α_i denote a fraction of total flow, the supply flow allocated to each groove is,

$$Q_{sup}^i = \frac{C_i}{C_{total}}Q_{sup}^{total} = \alpha_i Q_{sup}^{total}\bigg|_{i=1,\cdots,n} \tag{8}$$

7

Figure 6 depicts the predicted fraction of total supply flow $(\alpha_i)_{i=1,n}$ versus shaft speed and specific load for a four-pad TPJB[3] tested by Coghlan and Childs [5]. The bearing operates in a load between pad (LBP) configuration; the bottom two pads (#1 and #2) supporting the applied load. The dashed red line marks equal flow fractions (= ¼) for each pad at $W/(LD) = 0$ where the demand parameter $C_i \approx 1$ for all the grooves and hence each receives $(\alpha_i \approx 1/n)$ of the total flow.

As the load increases, the shaft eccentricity in the load direction increases and a small inlet film thickness restricts the flow for the loaded pads thus reducing (α_i), i.e. the demand of flow. On the other hand, a large film thickness on the unloaded pads requires more lubricant to create a full film, hence increasing α_i. Thus, the difference in flow fraction (α_i) for the loaded and unloaded pads grows as the applied load increases. The above-mentioned difference in flow demand is most significant between pad #3 and #1. One can surmise that during a high load operation the flow rate to pad #3 can be significantly reduced without substantial effect on the film temperature and overall bearing performance.

Figure 7 shows the flow fractions for a large size five-pad (LBP) TPJB[4] tested by Hagemann et al. [1]. Similar to the results in the prior figure, the loaded pads have a lower demand for supply lubricant compared to the unloaded ones. Notably, pad #2 (although unloaded) receives a small fraction of the total supply flow which is due to the large upstream flow leaving unloaded pad #1. Furthermore, an increase in shaft speed shifts the journal to a more centered position $(e \rightarrow 0)$, and (at a given load) slightly reduces the differences in flow demand.
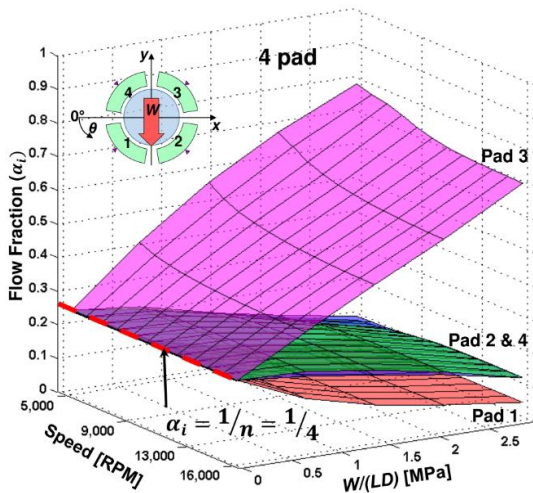

Figure 6: Predicted fractions of total supply flow (α_i) allocated to each groove in a 4-pad TPJB. (Dashed red line specifies an even distribution at zero load).
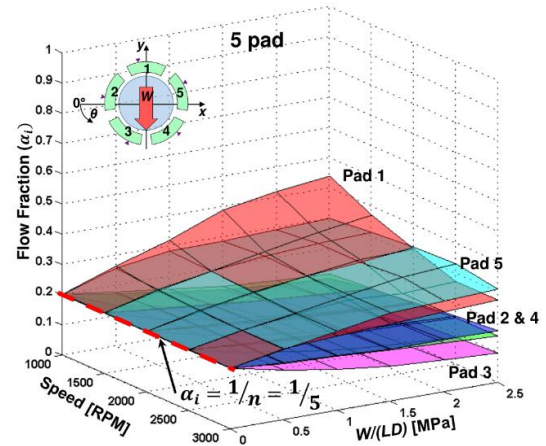
Figure 7: Predicted fractions of total supply flow (α_i) allocated to each groove for a 5-pad TPJB. (Dashed red line specifies an even flow distribution at zero load).

Figure 8 shows the lubricant flows and heat fluxes entering and exiting the boundaries of a control volume that represents a groove region. Cold lubricant is supplied into the bearing at a known flow rate (Q_{sup}^{i}) and temperature (T_{sup}). Hot oil leaving the trailing edge of the upstream pad with a flow rate (Q_{TE}^{i-1}) and a temperature (T_{TE}^{i-1}), loses some of its heat in the groove region and reaches the leading edge of the downstream pad with a flow rate (Q_{LE}^{i}) and a temperature (T_{LE}^{i}).

Based in Ref. [22], if $\left(Q_{TE}^{i-1} + Q_{sup}^{i}\right) > Q_{LE}^{i}$, the excess oil leaves the groove as a side leakage flow (Q_{SL}^{i}). Conversely, if the sum of the supply flow and upstream flow is not enough to fill in the downstream pad leading edge ($\left(Q_{TE}^{i-1} + Q_{sup}^{i}\right) < Q_{LE}^{i}$), then to satisfy the

---

[3] Refer to Table 4 for a description of the four-pad bearing in Ref. [5].

[4] Refer to Table 1 for a description of the five-pad bearing in Ref. [1]

continuity, the rest of the needed lubricant is drawn from the churning oil in the groove (Q_{gr}^i) [24]. According to the thermal mixing flow model in Ref. [24], for a groove with a non-zero side leakage flow (Q_{SL}^i), the groove recirculating flow is zero and vice versa.

$$Q_{SL}^i = Q_{TE}^{i-1} + Q_{sup}^i - Q_{LE}^i \qquad \text{if } \left(Q_{TE}^{i-1} + Q_{sup}^i\right) > Q_{LE}^i$$
$$Q_{gr}^i = Q_{LE}^i - Q_{TE}^{i-1} - Q_{sup}^i \qquad \text{if } \left(Q_{TE}^{i-1} + Q_{sup}^i\right) < Q_{LE}^i \qquad , \; i=1,..n$$
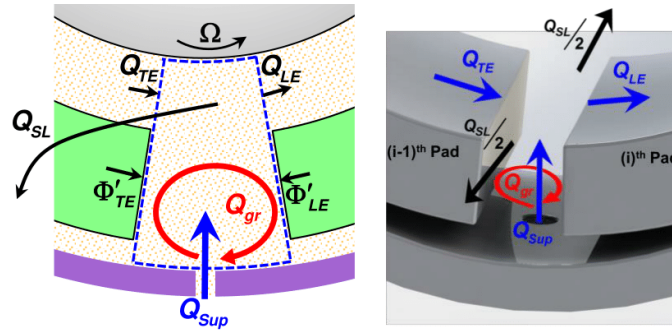
(9)

Figure 8: Mixing in a feed groove region of hot oil leaving an upstream pad (Q_{TE}^{i-1}) with a cold supply flow (Q_{sup}^i). Including side leakage flow (Q_{SL}^i) and groove recirculating flow (Q_{gr}^i) as well as heat transfer with the bounding pads.

Opposed to the conventional thermal mixing model in Eq. (1), the current model emphasizes the portion of hot oil that does not reach the next pad and either leaks out from the sides or recirculates within the groove. The temperature of the discharge side leakage flow (T_{SL}^i) and churning oil in the groove (T_{gr}^i) depend on the upstream oil temperature and flow rate $\left(T_{TE}^{i-1}, Q_{TE}^{i-1}\right)$ as well as supply temperature and flow rate $\left(T_{sup}, Q_{sup}^i\right)$.

In a bearing groove, thermal energy (heat) flows mainly by means of fluid motion, i.e. an advection heat transfer mechanism. Fluid flow (Q) transports energy from one location to another. The heat flow (Φ) transported by the lubricant is

$$\Phi = \rho c_p Q \Delta T$$

(10)

where ΔT is the temperature difference, and $\left(\rho c_p Q\right) = c_p \dot{m}$ is the fluid thermal capacitance.

Figure 9 shows two versions of the control volume at a groove, the left control volume refers to a situation where side leakage occurs, and the one on the right refers to a condition where oil streams recirculate in the groove. In both, heat flow (Φ) is transported internally by the mixing of the fluid streams. The left sub-control volume (bottom part) assumes that only a portion of the streams that flow into the groove (the hot upstream oil and the cold supply oil stream) carry the thermal energy that is transferred into the side leakage stream. Therefore, the heat flowing into the leading edge section of the downstream pad is omitted.

A mixing efficiency parameter ($0 < C_{gr} < 1$) represents the ability of a particular oil feed groove arrangement to lubricate the downstream pad with fresh (cold) supply oil while discharging the upstream hot oil (displacing it to the sides). That is, C_{gr} specifies the portion of the heat that flows from the hot upstream section $\left(\Phi_{TE,SL}\right)$ and the cold supply oil $\left(\Phi_{sup,SL}\right)$. Thermal energy must still be conserved within a sub control volume, thus the sum of two heat flows is nil, or $\left(\Phi_{TE,SL} + \Phi_{sup,SL}\right) = 0$.

Recall from Eq. (9), either the side leakage flow (Q_{SL}) or the groove churning flow (Q_{gr}) can be present in a groove, but not both. Hence, as shown on the right graph in Figure 9, only a portion of the fluid streams flowing into a groove contribute to transporting thermal energy to the oil stream that churns within the groove and therefore $\left(\Phi_{TE,gr} + \Phi_{sup,gr}\right) = 0$.
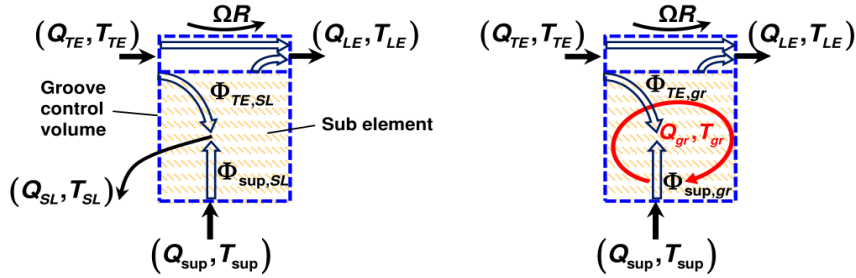
9

Figure 9: Groove control volume including fluid streams (solid arrows) and heat flows (hollow arrows). <u>Left</u>: heat flows from a hot upstream oil ($\Phi_{TE,SL}$) and the cold supplied oil ($\Phi_{sup,SL}$) into a stream that evacuates from the groove. <u>Right</u>: hot $\Phi_{TE, gr}$ and cold $\Phi_{sup,gr}$ flows into an oil stream that recirculates within the groove.

Conservation of energy dictates that the sum of the thermal energy transferred between the hot upstream oil and the side leakage oil ($\Phi_{TE,SL}$) and that between the side leakage oil and cold supplied oil ($\Phi_{sup,SL}$) equals zero, i.e.

$$\underbrace{C_{gr}\left[\rho c_p\, Q_{TE}^{i-1}\left(T_{TE}^{i-1}-T_{SL}^{i}\right)\right]}_{\Phi_{TE,SL}>0}+\underbrace{(1-C_{gr})\left[\rho c_p\, Q_{sup}^{i}\left(T_{sup}-T_{SL}^{i}\right)\right]}_{\Phi_{sup,SL}<0}=0 \tag{11}$$

From this balance, the temperature (T_{SL}^{i}) of the side leakage is

$$T_{SL}^{i}=\frac{C_{gr}\left[Q_{TE}^{i-1}\,T_{TE}^{i-1}\right]+(1-C_{gr})\left[Q_{sup}^{i}T_{sup}\right]}{\left[C_{gr}\,Q_{TE}^{i-1}+(1-C_{gr})\,Q_{sup}^{i}\right]};\; i=1,..,n \tag{12}$$

Note the oil volumetric heat capacity (ρc_p) is assumed not to change with temperature.

Direct lubrication methods such as a leading edge groove reduce hot oil carry over, which means the side leakage lubricant receives most of thermal energy form the hot upstream oil, and T_{SL}^{i} is closer to the upstream temperature (T_{TE}^{i-1}), hence $C_{gr}\to 1$. On the other hand, when the bearing axial ends are sealed (a flooded bearing) the hot upstream oil mixes with the cold supply oil before being squeezed out as a side leakage, hence $C_{gr}\to 0$.

<u>In the absence of any side leakage flow,</u> a similar transport energy balance establishes that the sum of the thermal energy transferred between a hot upstream trailing edge oil and the churning oil in the groove ($\Phi_{TE,gr}$) and that between the churning oil and a cold supply oil ($\Phi_{sup,gr}$) is zero. That is,

$$\underbrace{(1-C_{gr})\left[\rho c_p\, Q_{TE}^{i-1}\left(T_{TE}^{i-1}-T_{gr}^{i}\right)\right]}_{\Phi_{TE,gr}>0}+\underbrace{C_{gr}\left[\rho c_p\, Q_{sup}^{i}\left(T_{sup}-T_{gr}^{i}\right)\right]}_{\Phi_{sup,gr}<0}=0 \tag{13}$$

Hence, from Eq. (13), the temperature $\left(T_{gr}^{i}\right)$ of the recirculating oil in the groove is

$$T_{gr}^{i}=\frac{(1-C_{gr})\left[Q_{TE}^{i-1}\,T_{TE}^{i-1}\right]+C_{gr}\left[Q_{sup}^{i}\,T_{sup}\right]}{\left[(1-C_{gr})\,Q_{TE}^{i-1}+C_{gr}\,Q_{sup}^{i}\right]};\; i=1,..,n \tag{14}$$

The temperature of the churning oil in the groove (T_{gr}^{i}) is closer to T_{sup} if the majority of the hot upstream oil discharges from the sides ($C_{gr}\to 1$). However, for a flooded bearing a large portion of the upstream oil flow recirculates in the groove, thus increasing T_{gr}^{i} to a magnitude close to T_{TE}^{i-1} ($C_{gr}\to 0$). In other words, the larger the side leakage temperature (T_{SL}^{i}), the smaller the groove temperature (T_{gr}^{i}) and vice versa. Therefore, the groove temperature (T_{gr}^{i}) is the counterpart of the side leakage temperature (T_{SL}^{i}).

Some heat is also transferred from the wetted wall of the pad trailing edge and also from the wetted wall of a pad leading edge into the oil that is recirculating in the groove. These heat flows $\left(\Phi'_{TE}, \Phi'_{LE}\right)$ are obtained from integrating the convective heat fluxes across the respective fluid-solid boundary,

$$\Phi'_{LE} = h_{gr} L \int_{R_{back}}^{R_p} \left(T'_{(r,\theta_{LE})} - T_{gr}\right) dr; \quad \text{and}$$

$$\Phi'_{TE} = h_{gr} L \int_{R_{back}}^{R_p} \left(T'_{(r,\theta_{TE})} - T_{gr}\right) dr \qquad (15)$$

where L is a pad axial length and h_{gr} is the convection coefficient of the lubricant in the groove. See Abdollahi [20] for further details.

An energy balance method takes into account all the aforementioned heat fluxes to determine the film temperature at the leading edge of the downstream pad $\left(T^i_{TE}\right)$. Recall from Eq. (9) that Q^i_{gr} and Q^i_{SL} do not coexist (or apply simultaneously), only one is present at each groove (See later examples). The approach is energy conservative, namely at the ith groove

$$\underbrace{\rho c_p \left(Q^{i-1}_{TE} T^{i-1}_{TE} + Q^i_{sup} T_{sup} + Q^i_{gr} T^i_{gr}\right) + \Phi'_{TE} + \Phi'_{LE}}_{\text{Energy in}} = \underbrace{\rho c_p \left(Q^i_{LE} T^i_{LE} + Q^i_{SL} T^i_{SL}\right)}_{\text{Energy out}} \qquad (16)$$

Finally, from the above relation, the leading edge temperature (T^i_{TE}) of the fluid entering the ith pad is

$$T^i_{LE} = \frac{Q^i_{sup} T_{sup} + Q^{i-1}_{TE} T^{i-1}_{TE} - Q^i_{SL} T^i_{SL} + Q^i_{gr} T^i_{gr} + \left[\dfrac{\Phi'_{TE} + \Phi'_{LE}}{\rho c_p}\right]}{Q^i_{LE}} \qquad (17)$$

Unlike the conventional model, Eq. (1), the Eq. above includes the thermal energy from the side and churning fluid flows, as well as the heat convected from the pad metal surfaces into the lubricant. The above equations are easily integrated into a predictive model solving for the bearing pads hydrodynamic pressure and temperature fields, and including pad elastic deformations due to both mechanical (pressure) and thermal effects (expansion and crowning). See Ref. [20].

COMPARISON OF PREDICTIONS AGAINST TEST DATA

The following section presents two examples of analysis that demonstrate the validity of the novel model against test data reported in Refs. [1, 2]. The predictions account for both thermally and pressure induced deformation of the bearing components (TEHD model).

Large TPJB Operating at a High Surface Speed and Under a Heavy Load

Hagemann et al. [1] use a rig designed to test large size journal bearings for steam turbines. The shaft diameter is 500 mm (0.5 m) and the bearing length is 500 mm. The drive power (1.2 MW) enables operation with a shaft speed up to 4 kRPM (ΩR_s = 105 m/s). Spray bars deliver fresh (cold) lubricant to a test bearing. Two sealing baffles with a clearance of 1 mm (C/R_s = 0.004) at the axial ends of the bearing reduce the required supply flow rate to induce a flooded condition [1]. During the tests, the hollow rotating shaft with two piezoelectric pressure sensors and two capacitive displacement sensors is shifted axially to record the film thickness and pressure distribution over the full extent of the pad surfaces.

Table 1 outlines the geometry, lubricant properties, and operating conditions of one test bearing. Figure 10 shows a schematic view of the bearing and the load direction. For this test bearing, the length to diameter (L/D) = 0.7 and pad clearance to radius ratio (C_p/R_s) = 0.0012. Rocker back pivots, arched in the axial direction, enable the pads to also roll axially and reduce the influence of shaft misalignment. Refs. [1, 2] do not provide the pivot stiffness, however based on the geometry, a pivot stiffness is estimated using Hertz contact theory for a cylinder on a cylinder. The maximum applied load on the bearing is 1 MN; hence, the specific load ($W/(LD)$) ranges between 1 MPa and 2.5 MPa. Also, the large diameter of the rotor gives a surface speed between 13 m/s and 79 m/s for shaft speeds from 500 RPM to 3 kRPM.

Table 1: Characteristics of a test TPJB. Taken from Ref. [1]

| Bearing properties	
Load orientation	LBP
Number of pads	5
Shaft diameter [mm]	500
Pad thickness [mm]	72.5
Bearing axial length [mm]	350
Pad arc length	56°
Pivot offset	0.6
Pad clearance [μm]	300
Preload	0.23
Pad mass* [kg]	55.9
Pad moment of inertia about pivot point*	0.44
Pivot Stiffness* [N/m]	Hertz (~3 GN/m)
Operating condition	
Load [kN]	175–438
Specific Load $W / (L\,D)$ [MPa]	1–2.5
Shaft rotational speed [RPM]	500–3000
Shaft surface speed ΩR [m/s]	13–79
Lubricant supply temperature [°C]	50
Lubricant flow rate [L/min]	210 / 420
Fluid properties	
Lubricant	ISO VG32
Viscosity at supply temperature* [mPa·s]	22.4
Viscosity temperature coefficient* [1/°C]	0.0297
Density [kg/m3]	844
Specific heat capacity [kJ/(kg·K)]	2.17
Thermal conductivity [W/(m·K)]	0.13
Lubricant supply method	Spray-bar, Flooded
Thermal properties	
Pad and journal thermal conductivity	45
Sump temperature [°C]	65
Housing direction of expansion*	Outwards
Groove efficiency, C_{gr} (flooded)	0.2
∗Assumed based on the data in Ref. [1].	
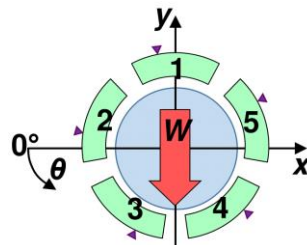
Figure 10: Schematic view of a five-pad TPJB in Ref. [1].

Figure 11 shows the pad surface temperature rise relative to the supply temperature (50°C) versus angle (θ). The measured pad temperatures are recorded using thermocouples located 5 mm behind the pad inner surface [1]. The novel thermal mixing flow model deliver results that are in good agreement with the test data, in particular for the unloaded pads. The current model improves the prediction of temperature as compared to the conventional model, Eq. (1) with λ=0.9. The pad leading edge temperature raises up to 17°C by accounting for the reduced supply flow rate in the test. The groove efficiency (C_{gr}) is selected as 0.2 since the bearing is flooded and a large portion of hot oil upstream of each groove presumably churns in the groove. Hence, the temperature of the recirculating lubricant in the groove (T_{gr}) is closer to the upstream temperature (T_{TE}) than to the oil supply temperature T_{sup}.
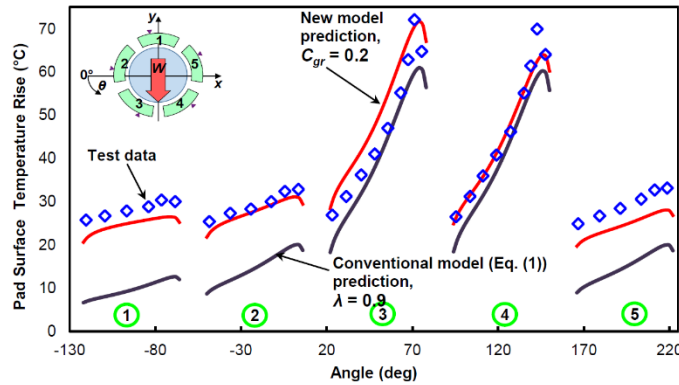

Figure 11: Pads' surface temperature rise versus circumferential location. Predictions from current and conventional oil thermal mixing models compared against test data in Ref. [1]. (Spray Bar, Flooded TPJB, T_{sup}= 50°C, N=3 kRPM, $W/(LD)$=2.5 MPa, and C_{gr} =0.2)

Table 2 compares the predicted flow rates from the current and conventional (early) thermal mixing models. The amount of flow needed to make up for the difference between the downstream flow (Q_{LE}) and the upstream flow (Q_{TE}) in the two models is almost the same[5].

The conventional model assumes the make-up flow only contains the supply of (fresh or cold) lubricant (Q_{sup}). The current model adds the churning oil in the groove (Q_{gr}) and side leakage flow (Q_{SL}) to the components of the make-up flow.

$$\text{Current model:} \quad Q_{LE} - Q_{TE} = Q_{sup} - Q_{SL} + Q_{gr}$$
$$\text{Conventional model:} \quad Q_{LE} - (\lambda Q_{TE}) = Q_{sup}$$

(18)

The conventional model predicts $\left(Q_{sup}^{total}\right)$ = 713 L/min, 70% more than the actual flow rate during the operation, that is just 420 L/min [1]. The present model allocates a percentage of the actual flow rate (420 L/min) to each groove based on the approximate flow

Table 2: Flow rates [L/min] in the feeding grooves of bearing in Ref. [1]. Predictions from current model (C_{gr}=0.2) and conventional model (λ=0.9). (Spray Bar, Flooded, N=3000 RPM, and $W/(LD)$=2.5 MPa)

Pad	Q_{TE}^{i-1}	Q_{LE}^{i}	α_i	Q_{sup}^{i}	Q_{SL}^{i}	Q_{gr}^{i}	Q_{sup}^{i}
	(L/min)			(L/min)			(L/min)
1	177	468	0.24	102	0	189	301
2	253	294	0.15	62	21	0	76
3	171	112	0.11	45	105	0	0
4	44	123	0.19	81	2	0	83
5	53	299	0.31	129	0	116	254
Total:			1	420 (L/min)=**Test**			713 (L/min)

Header spanning: "Current Model" spans α_i, Q_{sup}^{i}, Q_{SL}^{i}, Q_{gr}^{i}; "Conventional Model" spans the last column.

---

[5] The predicted Q_{LE}, Q_{TE} are only *slightly* different in the two models, due to distinct oil viscosity from different predicted film temperatures.

13

fraction (α_i), see Eq. (8). The rest of the lubricant required to fill in the pad inlet film thickness is drawn from the recirculating (churning) lubricant in a groove (Q_{gr}, T_{gr}).

Nicholas et al. [25] state that in a flooded TPJB design with a pressurized housing (not evacuated) "any additional oil that may be required is simply drawn from the captured oil inside of the bearing housing". Since the example bearing is flooded, a significant portion of the lubricant that leaves each pad (side or axially) is not immediately forced out of the bearing. Instead, it recirculates in the housing and provides the additional fluid required to fill in the film (Q_{gr})[6]. Note that the conventional model predicts a nil draw of supply lubricant for pad #3, whereas the current model predicts a significant side leakage flow (Q_{SL}) that discharges sideways off the groove.

Figure 12 shows the predicted pad inner surface temperature for two supply flow rates with operation at a shaft speed of 3 kPM and under a specific load of 1 MPa. Reducing the total supply flow rate means that more lubricant would be drawn from the grooves (larger Q_{gr}). While this is the case for a flooded bearing, excessive reduction in supply flow in an evacuated bearing induces oil starvation due to a lower availability of excess oil in the housing [25]. Note specifically the leading edge temperature for all of the examples which correlates well with the test data.
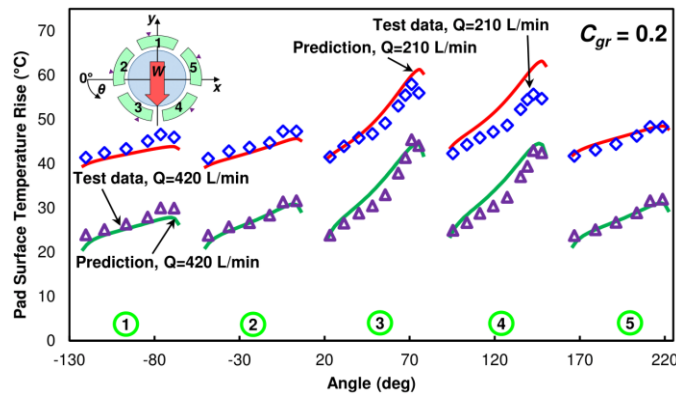

Figure 12: Pads' surface temperature rise versus circumferential location for two supply flow rates (210 L/min and 420 L/min). Predictions compared against test data in Ref. [1]. (Spray Bar, Flooded, T_{sup}= 50°C, N=3 kRPM, $W/(LD)$=1 MPa, C_{gr}=0.2)

Figure 13 compares temperatures predicted from the two thermal mixing models for operation at three shaft speeds. The predictions from the present mixing model keep the total supply flow rate constant (Q_{total} = 420 L/min), whereas the early thermal mixing model predicts $Q_{total} \approx$ 700, 1100, and 1650 L/min respectively for N = 1.5, 3, and 4.5 kRPM. The predicted temperatures from the conventional
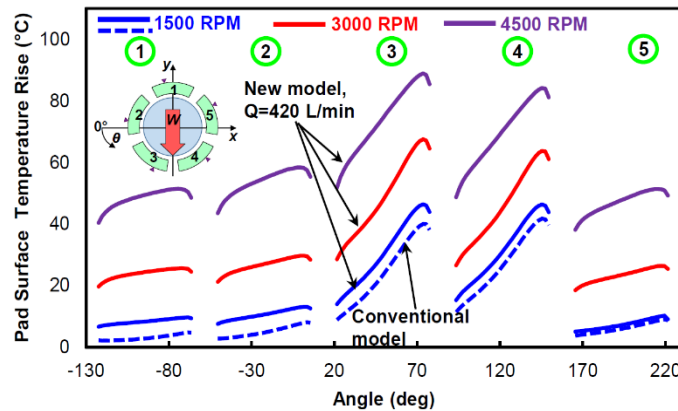

Figure 13: Pads' surface temperature rise versus angle for operation at three shaft speeds. (Spray Bar, Flooded, T_{sup}= 50°C, N=1.5, 3 and 4.5 kRPM, $W/(LD)$=2.5 MPa, C_{gr}=0.2, and λ=0.8)

---

[6] A flooded bearing requires less total (overall) supply oil compared to an evacuated one, since in an evacuated bearing all required lubricant must be solely supplied by the feed orifices (no recirculating flow). [25]

model are within 10 °C of each other; only one for $N = 1.5$ kRPM is shown. The predictions from the current model show a substantial increase in pad surface temperature with an increase in shaft speed.

The current model predictions for $N = 3$ kRPM are compared with test data shown in Figure 13. For a higher speed ($N = 4.5$ kRPM), however, the results may not be accurate since the amount of required groove flow (Q_{gr}) becomes very large and there may not be enough lubricant left (churning) in the bearing housing to provide it. In this situation, the full arc extent of the pads would not be lubricated which could induce oil starvation in one or more pads.

Table 3 compares the journal eccentricity along the load direction ($-e_y$) obtained with the novel thermal mixing model for both TEHD and THD model predictions[7]. The predicted journal eccentricity (e_x) in the orthogonal direction and the journal attitude angle ($\varphi = \tan^{-1}(e_x/e_y)$) are insignificant thus not shown. Hagemann et al. [1] do not report the test data for these parameters. The predicted journal eccentricity in the load direction delivered by the TEHD analysis is 25% to 30% smaller than that from the THD analysis. The difference decreases as the load increases since the eccentricity grows to nearly reach the cold (machined) pad clearance (300 μm).

Table 3: THD and TEHD predictions for journal eccentricity along the load direction (e_y) for four specific loads. ($N=3$ kPM, $C_{gr}=0.2$)

$W/(LD)$ [MPa]		1	1.5	2	2.5
THD	$-e_y$ [μm]	158	215	261	290
TEHD	$-e_y$ [μm]	112	151	186	216

Figure 14 shows the hydrodynamic pressure in the mid-plane of the bearing. The TEHD analysis, including thermal and mechanical deformations, shows very good agreement with the measurements. Neglecting the thermally induced deformation leads to under-predicting the pressure field, in particular its peak magnitude. Note the peak pressure TEHD prediction is[8] 5% larger than the measured magnitude, whereas the THD prediction is 27% smaller. The predicted hydrodynamic pressure shows a similar discrepancy with the test data for the lightly loaded pads (#1, #2, #5). See Ref. [20] for details on the thermal and pressure induced mechanical deformations.
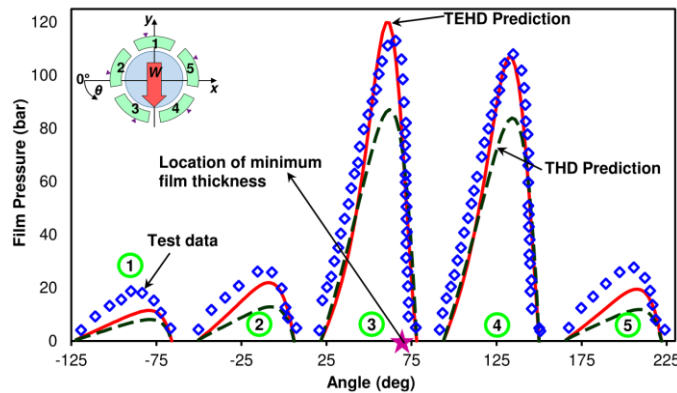

Figure 14: TEHD and THD predictions for mid-plane film pressure compared against test data in Ref. [1]. Star symbol (★) shows the location of minimum film thickness. ($N=3000$ RPM, $W/(LD)=2.5$ MPa)

Figure 15 shows the film thickness at the mid-plane of the bearing. The TEHD model including the thermal expansion of the pads, shaft and bearing housing delivers a smaller film thickness compared to that from the THD model. TEHD predictions have a slightly better agreement with test data for the minimum film thickness, ~ 10 μm. Note also the THD model does not accurately predict the slope of the film thickness with a significant difference (up to 45%) at the leading edge of the loaded pads (#3, #4). This is directly due to the pressure induced deformation (opening up) of these pads due to the applied load.

---

[7] In the following figures, 'TEHD' denotes thermo-elasto-hydro-dynamic that includes both thermally and mechanically induced deformation of the bearing components including pivot flexibility.

[8] The percentage of prediction difference compared to measured magnitudes is %Difference= (Measured-Predicted)/Measured.
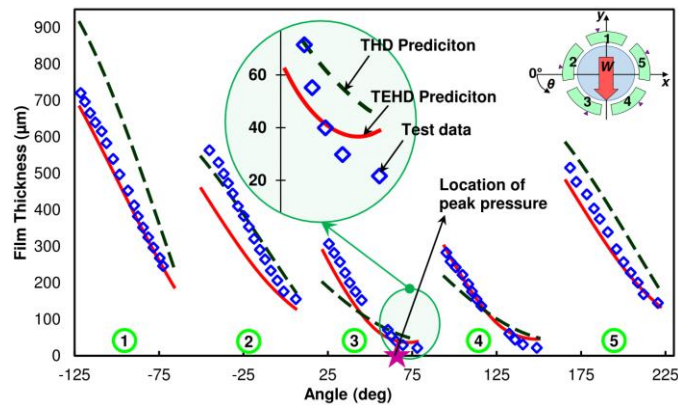
15

Figure 15: TEHD and THD predictions for mid-plane film thickness compared against test data in Ref. [1]. Star symbol (★) shows the location of peak pressure. (*N*=3 kRPM, *W/(LD)*=2.5 MPa).

Figure 16 shows the axial variation of the film pressure at the circumferential location where the peak hydrodynamic pressure on pad #3 occurs. Including the thermally induced deformation causes a considerable increase in peak film pressure, and a better agreement with test data. The peak pressure develops shortly before the minimum film thickness, at $\theta = 62°$ on pad #3 (see * in Figure 14).
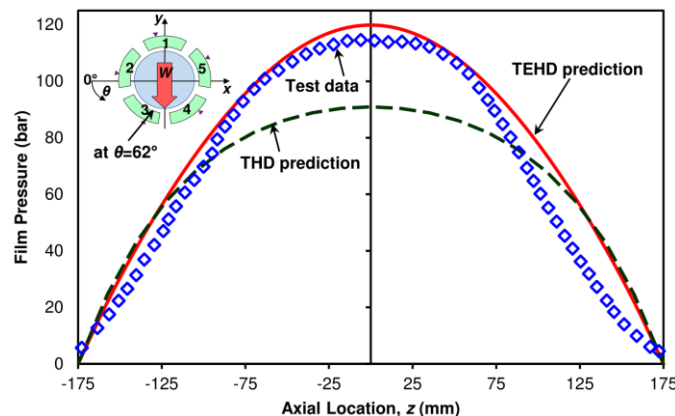
Figure 16: Predicted and measured film pressure at the circumferential location of peak pressure (θ=62°, see Figure 14). TEHD and THD predictions compared against test data in Ref. [1]. (*N*=3 kRPM, *W/(LD)*=2.5 MPa)

Figure 17 shows the axial variation of the oil film at its minimum thickness location, shortly downstream of the peak pressure location (θ=74°, see * in Figure 15). While prior research typically neglects the axial deformation of a pad, the test data shows that this deformation is actually significant. Modeling the axial deformations as a cantilevered beam model approximates the actual deformations with accuracy. Note also that the axial arch of the test bearing pivots contributes to the axial deformation of the pads.

The predicted film thickness at $z = \pm \frac{1}{2}L$ is about 25 µm lower than the measured magnitude which is about 8% of the cold pad clearance (300 µm). However, the axially averaged film thickness from the test data (49 µm) is very close to the one from the predictions (44 µm) which explains the accurate hydrodynamic pressure predictions.
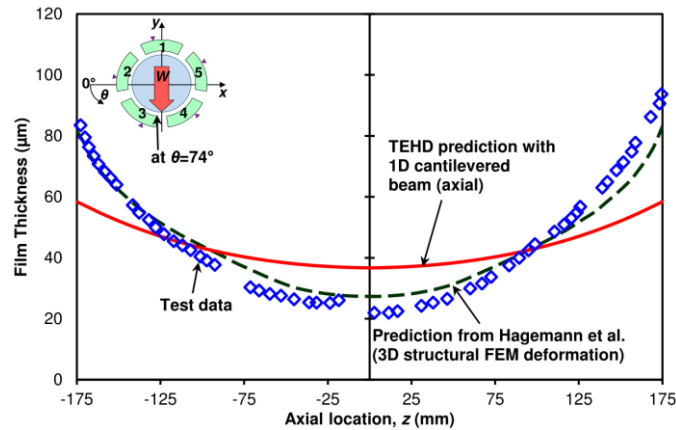
Figure 17: Predicted and measured film thickness in the circumferential location of the minimum film thickness (θ=74°, see Figure 15). Measured results in Ref. [1]. (N=3 kRPM, $W/(LD)$=2.5 MPa)

Figure 18 shows the bearing predicted direct stiffnesses (K) compared to the measurements and predictions in Ref. [2]. Predicted cross-coupled stiffnesses from the current model are much lower than the experimental magnitudes and not shown. For a specific shaft speed, the direct stiffnesses (K_{xx}, K_{yy}) increase with an increase in load.

The current predictions and those from Ref. [2] are greater than the measured stiffness coefficients. The prediction and measurements show the bearing is stiffer in the static load direction, or $K_{yy} > K_{xx}$. Unlike the predictions, the test data shows that stiffnesses reduce substantially for $N = 3$ kRPM compared to $N = 1.5$ kRPM. The stiffness orthotropy (difference between K_{yy} and K_{xx}) in the test data increases when rotor speed increases from $N = 1.5$ to 3 kRPM. The current model and Ref. [2], however, predict that the direct stiffness orthotropy reduces for operation at the high shaft speed (3 kRPM).
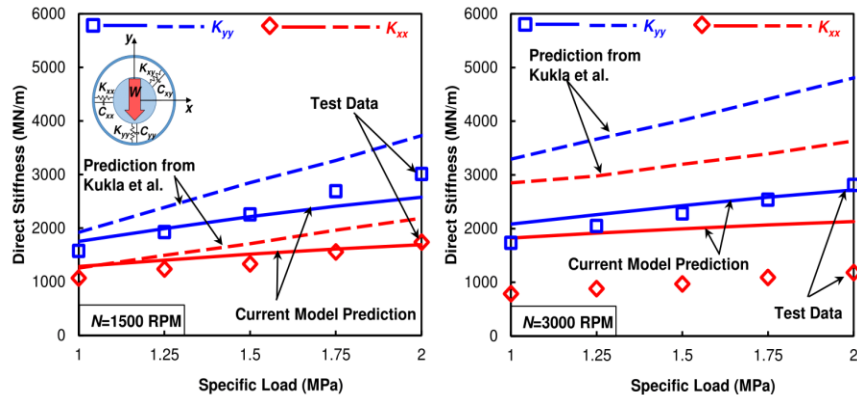

Figure 18: Direct stiffness coefficients (K_{yy}, K_{xx}) versus specific load for operation at two shaft speeds. TEHD prediction and test data in Ref. [2]. (Synchronous excitation; Left: N=1.5 kPM, Right: N=3.0 kRPM)

The agreement of the current TEHD predictions and the measured bearing stiffness in the load direction (K_{yy}) is very good. The maximum difference is less than 20% for operation at 1.5 to 3 kRPM. In the orthogonal direction, the difference for K_{xx} is up to 17% for $N = 1.5$ kRPM. However, at the high speed (3 kRPM) the predicted K_{xx} is twice the test data. Notably, an increase in shaft speed increases the estimated K_{yy} from test data, however sharply drops K_{xx} about 40%. This means shifting from an operation at $N = 1.5$ kRPM to $N = 3$ kRPM, the bearing stiffens along the load direction (y), whereas it softens in the orthogonal direction (x).

17

Figure 19 shows the predicted direct damping coefficients (C_{xx}, C_{yy}) compared to the test data and predictions in Ref. [2]. Predicted cross coupled terms are one order of magnitude smaller than the test data and not shown. The predicted C_{xx}, C_{yy} are consistently smaller than the estimated ones from test data. Contrary to the test data and predictions in Ref.[2], the current model predicts that direct damping decreases with an increase in applied load. The current predictions have a considerable discrepancy with the test data; between 33% and 53% for $N = 1.5$ kRPM and between 48% and 68% for $N = 3$ kRPM. The flexible pivot with a stiffness smaller than the film stiffness is likely accountable for the significant reduction in the predicted bearing damping.
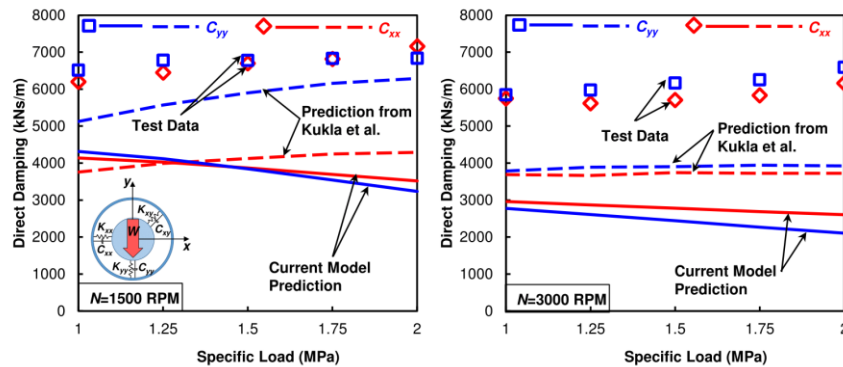

Figure 19: Direct damping coefficients (C_{yy}, C_{xx}) for operation at two shaft speeds. Prediction and test data from Ref. [2]. (Synchronous excitation; Left: N=1.5 kRPM, Right: N=3.0 kRPM)

The results above (Figures 18-19) are of interest due to the large deviation between the predictions and the test results. Kukla et al. [2] assert that no fundamental error occurred in their analysis or test procedure (although their own predicted dynamic force coefficients do not correlate well with the test data). Note that the test procedure in Ref. [2] is not conventional as the dynamic force coefficients are calculated from the measured film pressure. The authors state the key problem in the test procedure is neglecting pad inertia effects on identifying force coefficients. Kukla et al. [2] also believe that neglecting the axial shifting of the shaft in the support bearings and its dynamic behavior may have affected the test results.

Spherical Seat TPJB Under Heavy Specific Load and High Speed

Coghlan and Childs [3-5] conducted an extensive test program to study the effects of various lubrication (oil feed) configurations on the static and dynamic force performance of a spherical seat TPJB. The authors performed measurements for various lubrication delivery configurations, as shown in Figure 20.

- Flooded single-orifice (SO), labyrinth end seals with nominal clearance of 170 µm
- Evacuated leading edge groove (LEG), no end seals
- Evacuated spray-bar (SB), no end seals
- Evacuated spray-bar blocker (SBB), no end seals

Coghlan and Childs measured pad surface temperature (embedded in the Babbitt layer), journal eccentricity, hot bearing clearances, and a complex stiffness for each feeding arrangement and for operation with a shaft speed ranging from 7 kRPM and 16 kRPM ($\Omega R_s = 85$m/s), and under a specific load, 0.7 MPa to 2.9 MPa. The authors then curve fit a frequency independent ([K, C, M]) model to the complex stiffnesses data to extract the stiffness (K), damping (C), and virtual mass (M) coefficients of the bearing.
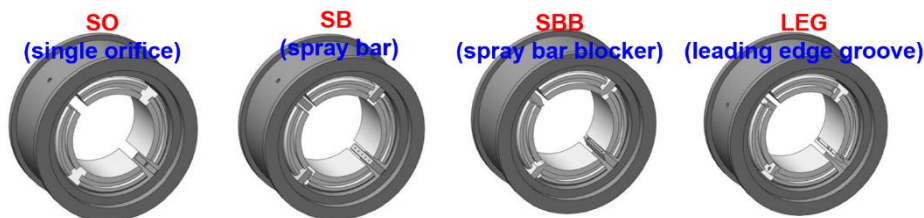

Figure 20: Schematic of lubrication delivery methods. Reproduced with permission from Ref. [5]

18

Table 4: Characteristics of a TPJB tested by Coghlan and Childs [3].

| Bearing properties	
Load orientation	LBP
Number of pads	4
Shaft diameter [mm]	101.59
Pad thickness [mm]	19
Bearing axial length [mm]	61
Pad arc length	72°
Pivot offset	0.5
Pad clearance [μm]	134
Preload	0.3
Pad mass* [kg]	0.6
Pad moment of inertia about pivot point*	0.46×10^{-4}
Pivot Stiffness* [N/m]	4.12×10^{8}
Operating condition	
Load [kN]	4.3–17.7
Specific Load $W/(L\,D)$ [MPa]	0.7–2.9
Shaft rotational speed [RPM]	7000–16000
Shaft surface speed ΩR [m/s]	38–85
Lubricant supply temperature [°C]	49
Lubricant flow rate [L/min]	38(Flooded) / 42
Fluid properties	
Lubricant	ISO VG46
Viscosity at supply temperature* [mPa·s]	25.6
Viscosity temperature coefficient* [1/°C]	0.0431
Density [kg/m3]	843.5
Specific heat capacity [kJ/(kg·K)]	2.084
Thermal conductivity [W/(m·K)]	0.1243
Thermal properties	
Pad and journal thermal conductivity	52
Sump temperature [°C]	51-64
Housing direction of expansion*	Outwards
Groove efficiency, C_{gr} (spray bar)	0.6
*Assumed based on the data in Ref. [3]	
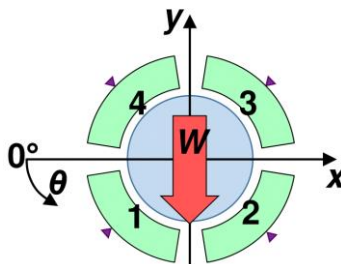
Figure 21: Schematic view of a four-pad TPJB in Ref. [3].

The following predictions pertain to a TPJB with spray bars (SB) delivering the supply oil and having no end seals (retainers) to evacuate the housing from recirculating lubricant. Buffer seals prevent oil axial leakage from the test bearing into the adjacent support

bearing chambers and guide it to oil outlet pipes. The authors selected (based on industrial practice) the location to measure the maximum temperature at 75% of the pad arc length. All thermocouples are type J with a measurement error of ±1 °C.

Figure 22 shows the pad surface temperature for operation at 7 kRPM shaft speed (37 m/s) and under three magnitudes of specific load (along y direction); 0.7 MPa to 2.9 MPa. Following the bearing provider recommendation, the flow rate is fixed at 42 L/min suitable for the highest shaft speed (16 kRPM) during all the test operating conditions. Hence, the bearing is over-flooded at 7 kRPM causing substantial amounts of fresh lubricant to axially discharge from a groove. A groove efficiency C_{gr} = 0.6 delivers pad surface temperature predictions agreeing with the test data for the TPJB equipped with spray bars. Since the known supply flow rate is utilized to obtain the predictions using the novel oil thermal mixing model, a constant C_{gr} provides accurate pad surface temperatures.
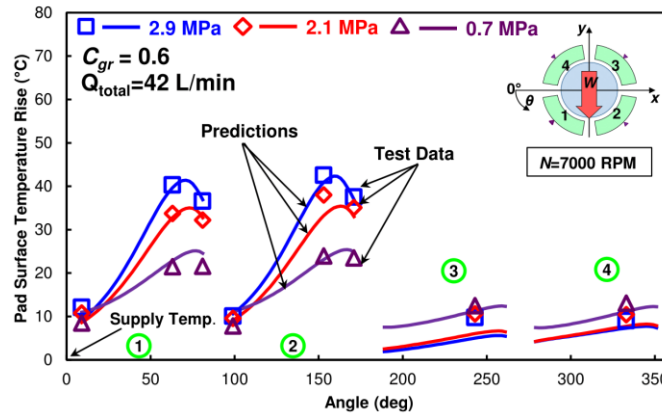

Figure 22: Pads' surface temperature rise versus circumferential location. Predictions compared against test data in Ref. [3]. (Spray Bar, Evacuated, T_{sup}= 49°C, N=7 kRPM, $W/(LD)$= 0.7, 2.1, 2.9, MPa, and C_{gr}=0.6)
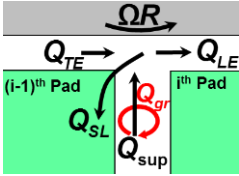
The agreement between the predictions (TEHD) and the measurements is remarkable; the largest temperature difference amounts to less than 3 °C for all three loads. As expected, the loaded pads are hotter for operation with a large specific load (2.9 MPa). Conversely, the unloaded pads (#3, #4) are hotter when operating with a small specific load (0.7 MPa). This phenomenon appears both in measurements and predictions. For (loaded) pads #1 and #2, the predicted temperatures are generally close to the measurements; conversely, the measured temperatures on (unloaded) pads #3 and #4 are higher than the predictions.

Table 5 shows the predicted flows in the groove region delivered by the current and conventional oil thermal mixing models for operation at a low speed (N = 7 kRPM) and a low specific load ($W/(LD)$ = 0.7 MPa). Note the large amounts of side leakage flow (Q_{SL}) and absence of groove flow (Q_{gr}) predicted by the current model as the bearing is evacuated (without end seals). The conventional thermal mixing model predicts Q_{sup}^{total} = 19 L/min since it does not account for the excessive supplied oil (42 L/min). The current model sets Q_{sup}^{total} = 42 L/min, and calculates the amount of extra supplied oil that leaves the groove as a side leakage (Q_{SL}).

Pad #3 (unloaded) demands 41% of the supplied oil (42 LPM) since it receives a diminished flow from upstream pad #2. On the other hand, (loaded) pad #1 demands the least amount of supply oil as it is immediately after an unloaded pad (#4).

Nicholas et al. [25] suggest that in an evacuated bearing, depending on the effectiveness of the lubricant supply mechanism, some oil escapes the bearing directly without ever lubricating the pads. The temperature of the side leakage flow (T_{SL}) is therefore predicted from a weighted average between the hot upstream flow and the supply flow temperatures adjusted by the groove efficiency parameter (C_{gr}), as given by Eq. (13).

Table 5: Flow rates [L/min] in the feeding grooves of bearing in Ref. [3]. Predictions from current model (C_{gr}=0.6) and conventional model (λ=0.8). (Spray Bar, Evacuated, $W/(LD)$=0.7 MPa, N=7 kRPM)

Pad	Q_{TE}^{i-1}	Q_{LE}^{i}	α_i	Q_{sup}^{i}	Q_{SL}^{i}	Q_{gr}^{i}	Q_{sup}^{i}
				Current Model			**Conventional Model**
	(L/min)			(L/min)			(L/min)
1	7.0	6.2	0.14	5.8	6.7	0	0.6
2	3.5	6.2	0.23	9.7	7.0	0	3.4
3	3.5	10.6	0.41	17.2	10.1	0	8.7
4	7.1	10.6	0.22	9.4	5.8	0	5.3
		Total:	1	42 (L/min) =**Test**			19 (L/min)

Figure 23 shows the pad surface temperature predictions and measurements recorded in the bearing operating at a high speed (16 kRPM) and under three static loads. Note the difference between predictions and test data for the loaded pads (#1,#2) does not exceed 4 °C. The predicted temperatures for the unloaded pads have a slightly larger discrepancy with the test data, up to 10 °C. Since the bearing operates in an evacuated condition, it is likely that the unloaded pads are not fully wetted. Yet the predictions are based on the assumption that each pad has a continuous fluid film.
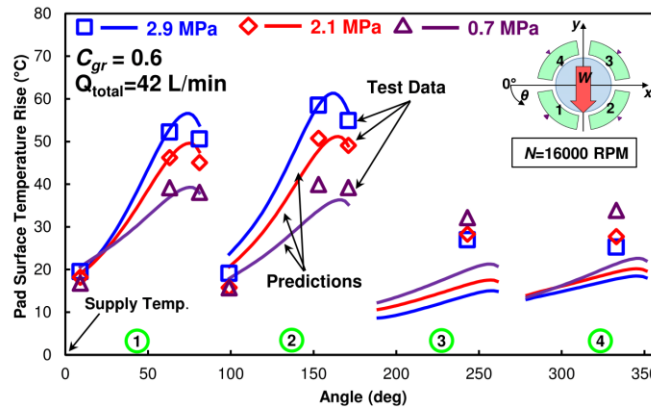

Figure 23: Pads' surface temperature rise versus circumferential location. Predictions compared against test data in Ref. [3]. (Spray Bar, Evacuated, T_{sup}= 49°C, N=16 kRPM, $W/(LD)$= 0.7, 2.1, 2.9, MPa, and C_{gr}=0.6).

Table 6 shows the predicted flows in the groove region from the current and conventional thermal mixing models for an operation at a high speed (N = 16 kRPM) and high specific load, $W/(LD)$ = 2.9 MPa. The conventional model predicts a total supply Q_{sup}^{total} = 48 L/min, slightly larger than the actual test condition (42 L/min). For the first pad, $Q_{TE}^{i-1} > Q_{LE}^{i}$, thus the conventional model predicts a nil supply flow rate.

Conceivably, a portion of the extra lubricant coming from the upstream unloaded pad #4 axially discharges as a side leakage and does not enter pad #1. The novel thermal mixing model predicts the large side leakage flow (Q_{SL}^{1} = 14.6 L/min). On the other hand, a large magnitude of groove flow (Q_{gr}^{4} = 4.3 L/min) for an evacuated bearing is not physically achievable and suggests occurrence of oil starvation. In this situation, the available supply flow (5.7 L/min) is not enough to create a full film at the pad #4 leading edge; thus, a full film develops further along the pad arc length. See Ref. [26] details on a flow starvation model that uses an effective pad arc (wetted) length.

As shown in Table 6, unloaded pad #3 demands the majority (66%) of the supplied flow, while the flow for loaded pad #1 reduces to just 6%. This is due to a highly eccentric journal position produced by a high 2.9 MPa specific load. Pad #2 (loaded) and pad #4 (unloaded) equally demand 14%; one pad receives the least amount of hot oil carry over, while the other receives the most.

21

Table 6: Flow rates [L/min] in the feeding grooves of a bearing in Ref. [3]. Predictions from current model (C_{gr}=0.6) and conventional model (λ=0.8). (Spray Bar, Evacuated, $W/(LD)$=2.9 MPa, N=16 kRPM)

Pad	Q_{TE}^{i-1}	Q_{LE}^{i}	α_i	Q_{sup}^{i}	Q_{SL}^{i}	Q_{gr}^{i}	Q_{sup}^{i}
	(L/min)			(L/min)			(L/min)
1	22.6	10.3	0.06	2.4	14.6	0	0
2	3.9	9.7	0.14	6.0	0.3	0	7.1
3	3.4	31.2	0.66	28.0	0.1	0	27.8
4	22.8	32.7	0.14	5.7	0	4.3	13.3
		Total:	1	42 (L/min) =**Test**			48 (L/min)

Figure 24 compares the maximum predicted pad #2 surface temperature to the measured one for various operating conditions, versus speed and load. A fixed groove efficiency parameter (C_{gr} = 0.6) delivers predicted temperatures that best fit the test data for all operating conditions with a maximum discrepancy up to 4 °C.
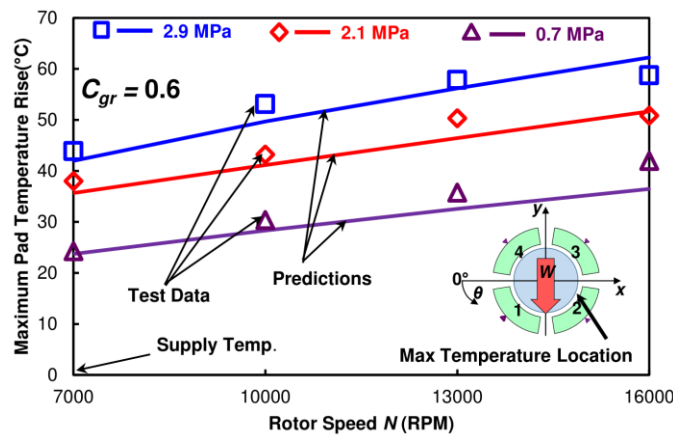

Figure 24: Maximum inner surface temperature on pad #2 versus shaft speed and for specific load, $W/(LD)$=0.7, 2.1 and 2.9 MPa. Current predictions and test data in Ref. [3].

The ability to accurately predict the temperatures with a single C_{gr} is a notable improvement over the earlier thermal mixing model in which the hot oil carry over factor (λ) needs to be tailored for each operation (in particular shaft speed). Recall that during the tests reported in Ref. [3], the total supply flow rate is kept constant (42 LPM) for all operating conditions.

Figure 25 shows the predicted total flow rate produced by the conventional oil mixing thermal model with $\lambda = 0.8$ versus shaft speed for three specific loads. For most operating conditions, the predicted total supply flow rate is less than the actual one. During the tests, the excess supply flow likely discharged axially from the bearing grooves (wide open seals) and did not lubricate the pads. However, the excess flow contributes to reducing the temperature of the hot oil that travels across each groove. Since the conventional model does not account for side leakage flow, a smaller[9] λ must be selected for low shaft speeds to fit the predicted temperatures to the test data. The current thermal mixing model, as shown in Figure 24, delivers accurate film temperatures for a range of operating conditions with a fixed total supply flow using a constant C_{gr}.

---

[9] From Eq. (1) $Q_{sup} = Q_{LE} - \lambda\, Q_{TE}$; a decrease in λ produces an increase in the predicted supplied flow.

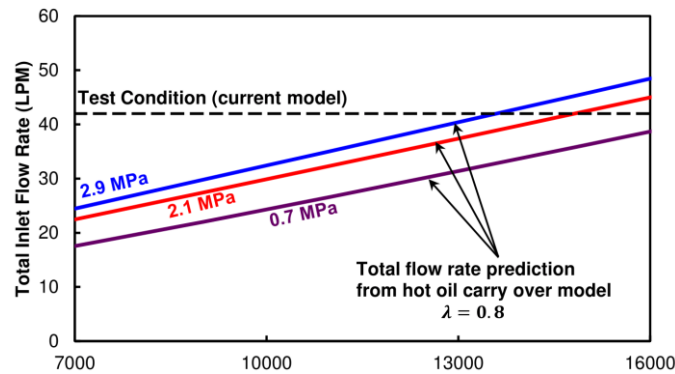**Figure 25: Predicted flow rate versus shaft speed and specific load *W/(LD)*=0.7, 2.1, 2.9 MPa. Conventional thermal mixing model (*λ*=0.8). Constant flow rate in tests [3] for spray-bar with evacuated housing.**

Figure 26 compares the predicted pad surface temperature and test data for the other three lubricant delivery methods, namely leading edge groove (LEG), spray bar blocker (SBB), single orifice (SO). The influence of a feeding arrangement on the overall temperature of the film and bounding solids is not limited to the leading edge temperature of the pads. A feeding arrangement alters the temperature generation in the film, the convection coefficients on the pad surfaces, the pressure boundary condition at a pad's leading edge, the turbulence intensity of the supply flow, etc. [27, 28]. However, by selecting an efficiency parameter (C_{gr}) appropriate for the feeding arrangement one can fairly predict the overall film temperature for the various delivery methods[10].
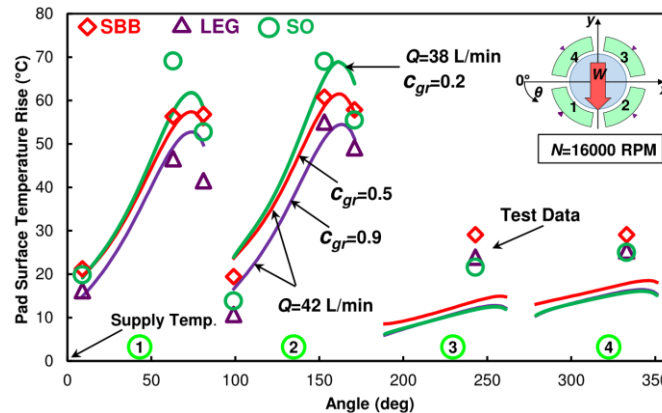

Figure 26: Pads' surface temperature rise versus circumferential location for three lubricant delivery methods. Predictions compared against test data in Ref. [5]. (SBB=Spray Bar Blocker, LEG=Leading Edge Groove, SO=Single Orifice, T_{sup}= 49°C, *N*=16 kRPM, *W/(LD)*=2.9 MPa)

Predicted pad temperatures with $C_{gr} = 0.9$ and 0.5 correlate best with the test data for LEG and SBB (evacuated spray-bar blocker) lubricant delivery methods, respectively. A spray bar blocker design includes a scraper to remove a layer of the upstream hot oil and displace it out of bearing more effectively compared to a conventional spray bar. However, in Ref. [5] the measured peak temperature of each pad with a SBB feeding configuration is higher than that with a SB (evacuated spray-bar) configuration. Coghlan [5] explains "the SBB attempts to scrape away the hot oil and in doing so seems to back-up the hot oil onto the upstream pad increasing the trailing edge temperatures."

The bearing with a single orifice (SO) feeding arrangement is flooded (as it has end-seals) and receives $Q_{sup}^{total} = 38$ L/min during the tests. Predicted temperatures with a $C_{gr} = 0.2$ match the maximum pad temperature, but show about a 10 °C discrepancy with the test data for the leading edge temperature of pad #2. In fact, the measurements in Ref. [5] consistently suggest that the pad leading edge

---

[10] Refer to Table 7 (Conclusion) for a recommended range of groove efficiency parameter (C_{gr}) applicable to various lubricant feeding arrangements.

temperature in a SO configuration is lower than that of SB and SBB (not LEG though), alas the maximum measured temperature for the SO bearing configuration is always the largest.

Figure 27 shows the predicted journal eccentricity along the load ($-y$) direction compared to the measurements in Ref. [3]. Coghlan and Childs [3] introduce a novel method to measure the journal eccentricity by defining a hot bearing center. The new hot bearing center is the origin of a circle that best fits the measured bearing clearances for each pad immediately after an operational shut down. The conventional definition of the hot bearing center is the position of the journal with a zero applied static load, and which is also used in the current predictive model.

The TEHD predictions follow the trend of the test data but with a more or less constant difference which is likely due to the unconventional definition of the bearing center (origin) for the test data. In the load direction ($-e_y$), the agreement between prediction and test data worsens by increasing the specific load. Predicted journal eccentricities from the TEHD analysis (solid lines) correlate best with the test data, but are ~25% smaller than the predictions from the THD analysis (dashed lines). The maximum difference between TEHD predictions and test data is 12, 29, and 37 µm for specific load $W/(LD)$ = 0.7, 2.1, and 2.9 MPa, respectively.

The predicted journal eccentricity in the orthogonal direction (e_x, not shown) does not exceed 3 µm while the measured ones range between 3 µm and 20 µm. Coghlan [5] states the significant measured orthogonal eccentricity indicates that the tilt motion of the pads is impeded by (unquantified) friction between a pad and its spherical seat pivot.
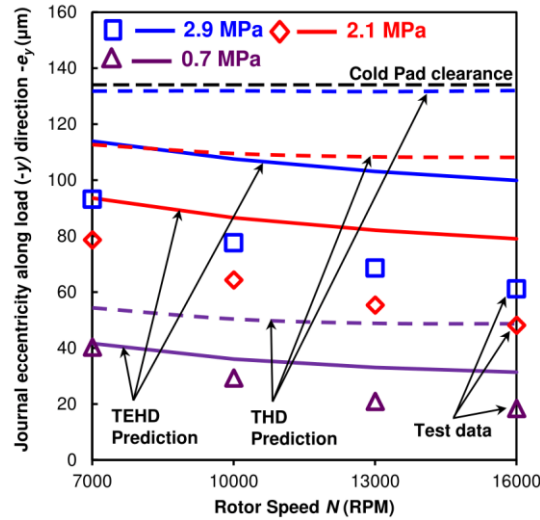

Figure 27: Journal eccentricity ($-e_y$) versus rotor speed and specific load $W/(LD)$=0.7, 2.1, 2.9 MPa. Predictions and test data in Ref. [5].

Coghlan and Childs [4] use a frequency independent [K, C, M] model to extract the bearing static stiffness [K], viscous damping [C], and virtual mass [M] coefficients from curve fits to the experimentally derived complex stiffnesses [H]. The imaginary part of the complex stiffness is approximately linear and the slope defines the bearing damping, i.e. $\Im(H) \Rightarrow \omega C$. The magnitude of complex stiffness real part at zero excitation frequency is the bearing stiffness and a quadratic curvature represents the bearing virtual mass, i.e. $\Re(H) \Rightarrow K - \omega^2 M$. H is identified over the frequency range 10 to 250 Hz. See Ref. [4] for details on the tests and identification procedure delivering:

$$\Re(H) \Rightarrow \left(K - \omega^2 M\right), \Im(H) \Rightarrow \left(\omega C\right) \tag{19}$$

Figure 28 and 29 show the real and imaginary parts of *H* as well as the TEHD predictions for operations at two shaft speeds, 7 kPM and 16 kRPM. Each figure reports data for specific load *W/(LD)*=0.7, 2.1, 2.9 MPa. The right side of the figures show the real part of the bearing direct complex stiffnesses ($\Re(H)$), and the left part shows the imaginary part ($\Im(H)$) versus excitation frequency.

The predicted $\Re(H)$ shows good agreement with test data for the shown operating conditions. The predicted $\Im(H)$ follows the test data closely at N = 7 kRPM, but the agreement reduces as either the shaft speed or the static load increases. The predictions are identical in the load (*y*) or orthogonal (*x*) directions. However, both the imaginary and real parts of the test *H* are larger along the load direction, and the difference increases as the specific load increases. Since the predictions are the same along the *x* and *y* directions, and under-predict the test data, they correlate best with the real and imaginary parts of H_{xx}.
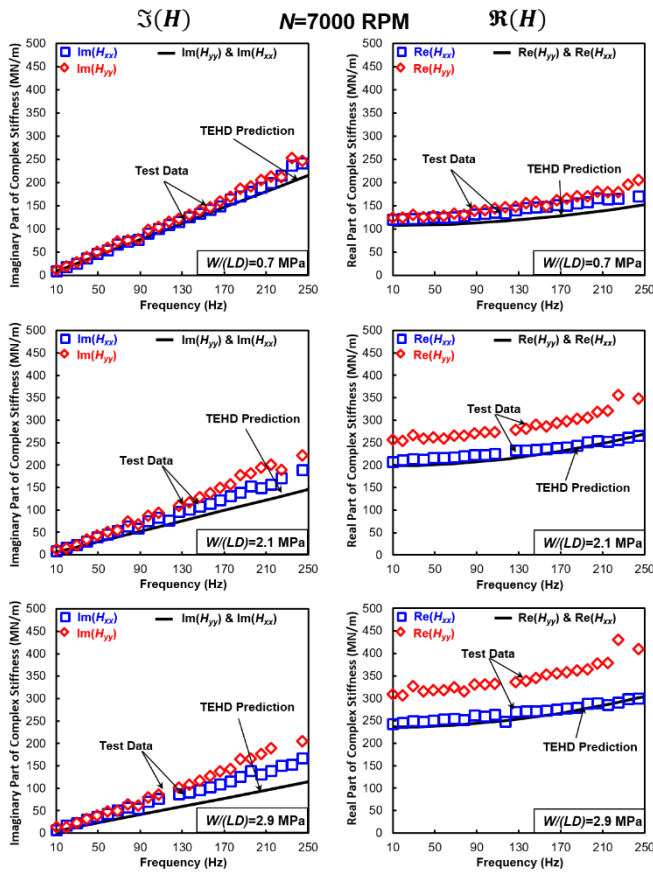

Figure 28: Imaginary (left) and real (right) parts of bearing complex stiffness (*H*) versus excitation frequency. TEHD predictions and measurements in Ref. [4] for operation of *N*=7 kRPM, and *W/(LD)*=0.7, 2.1, and 2.9 MPa.
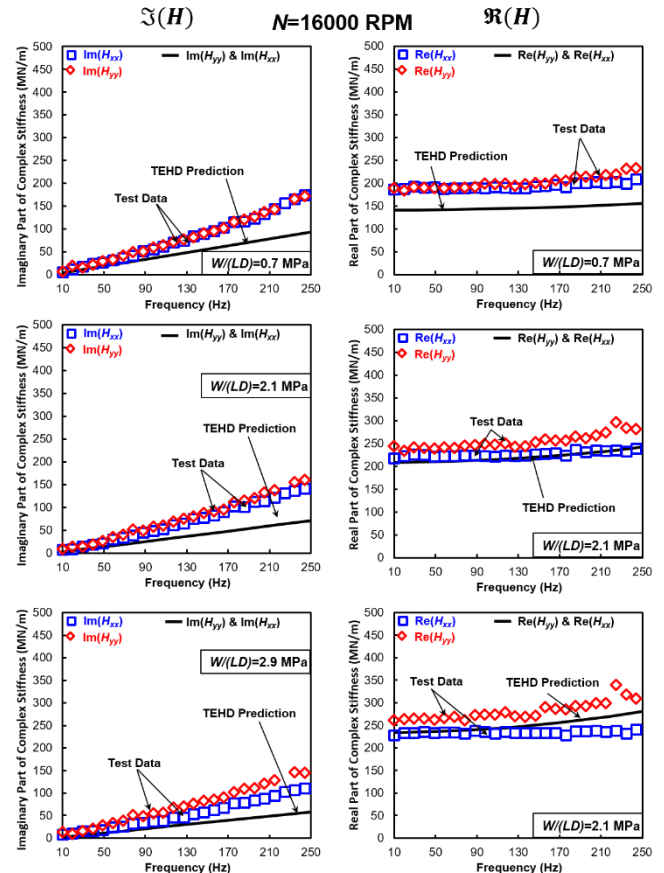
Figure 29: Imaginary (left) and real (right) parts of bearing complex stiffness (*H*) versus excitation frequency. TEHD predictions and measurements in Ref. [4] for operation of *N*=16 kRPM, and *W/(LD)*=0.7, 2.1, and 2.9 MPa

Figure 30 shows the measured and predicted bearing direct force coefficients (stiffness, damping, and virtual mass) versus specific load, 0.7 MPa to 2.9 MPa, for shaft speeds ranging between 7 kRPM and 16 kRPM. The uncertainty associated with the measured direct stiffness and damping are 2% and 5% of the coefficient magnitude, respectively. The predicted cross-coupled force coefficients are very small and not shown. The predictions include a linear pivot stiffness of 412 MN/m, as reported in Ref. [5], and which is in the same order of magnitude as the predicted film stiffness with a rigid pivot assumption (150 MN/m to 700 MN/m).

Figure 30 depicts that the bearing stiffnesses (K_{xx}, K_{yy}) increase with an increase in the static load at a given shaft speed. On the other hand, an increase in shaft speed reduces the bearing stiffness (K_{xx}, K_{yy}) at a constant specific load. The model predicts isotropic stiffnesses ($K_{xx} = K_{yy}$) but the test data show significant orthotropy ($K_{yy} > K_{xx}$), and which is not expected for a LBP configuration with

25

identical pads. Also, the stiffness orthotropy in the test data increases with an increase in specific load. Predicted K_{yy}, K_{xx} are in a good agreement with the measurements with a maximum difference not exceeding 25%, with an average difference of 17% along the load direction (y) and 8% in the orthogonal direction (x).
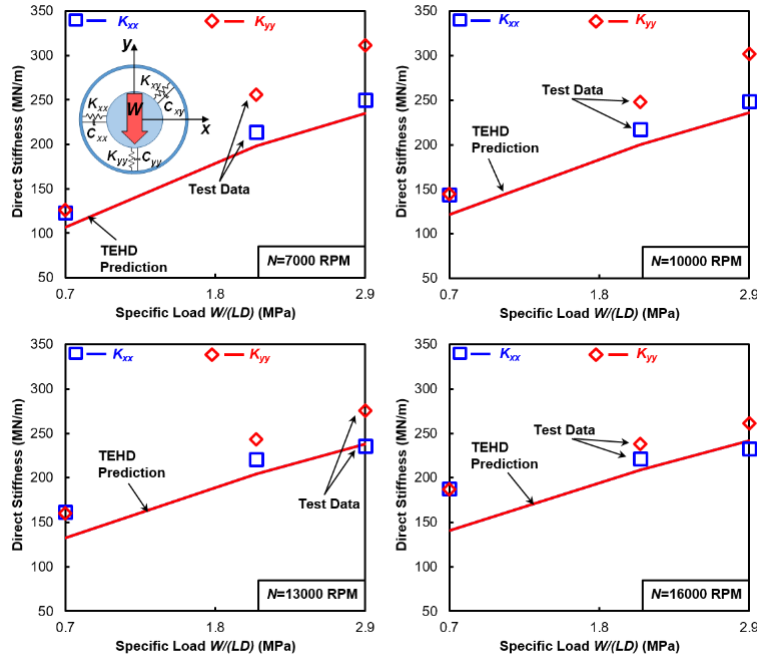

Figure 30: Direct stiffness coefficients (K_{yy}, K_{xx}) versus specific load for operation at four shaft speeds, 7 kRPM to 16 kRPM. TEHD prediction and test data in Ref. [4].

Figure 31 shows predicted damping coefficients (C_{xx}, C_{yy}) in comparison with the test derived coefficient. The bearing damping decreases with an increase either in the static load or the shaft speed. As the shaft speed or specific load increase, the predicted damping coefficients decline more rapidly compared to test data. Compared to the stiffnesses, the predicted (C_{xx}, C_{yy}) show a consistent large discrepancy with the measurements. The maximum difference between predictions and test data is 59% and 45% for C_{yy} and C_{xx}, respectively. The average difference is 25% in the load direction and 41% in the orthogonal direction with respect to the test data.

Judging from the similar trends in the TEHD predictions and the test data for stiffness and damping coefficients and observing a consistent difference, it is surmised that the pivot stiffness (412 MN/m) used in the predictions is not sufficiently large. The discrepancy between the predicted damping coefficients and the test data is more pronounced than that for the stiffnesses since "Pivot flexibility has a more pronounced effect on reducing the bearing damping coefficients than the stiffness coefficients" [17].

According to Coghlan [5], the pivot stiffness is approximated by fitting a linear curve to force versus displacement data for a single pad in LOP orientation. The range of the applied force to measure pivot stiffness is up to 4,750 N. During the tests, however, the applied load on the bearing ranges up to 18,000 N. It is not clear if the pivot stiffness remains the same in an operation under a heavy load and high oil temperature. Furthermore, Harris [29] details the complexities associated with measuring the stiffness of a similar spherical seat pivot, such as machining tolerance that makes the pivots non-identical, and the differential thermal growth of a steel ball and its bronze socket.

Figure 32 shows predicted virtual mass coefficients (M_{xx}, M_{yy}) in comparison with the test force coefficients. A negative virtual mass indicates that the real part of the complex stiffness ($\Re(H)$) increases with excitation frequency. This 'hardening effect' is common in TPJBs [5]. Unlike the bearing stiffness and damping from the test data, the test identified virtual mass magnitudes carry a significant uncertainty (sometimes up to 50%) associated with them. Hence, one cannot rely on the exact magnitudes of the reported test virtual mass.
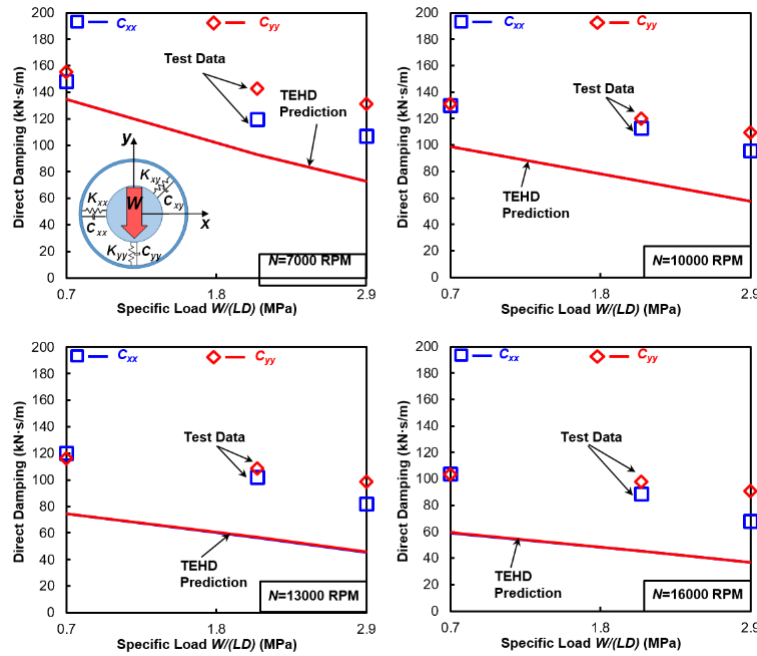
Figure 31: Direct damping coefficients (C_{yy}, C_{xx}) versus specific load for operation at four shaft speeds, 7 kRPM to 16 kRPM. TEHD prediction and test data in Ref. [4].
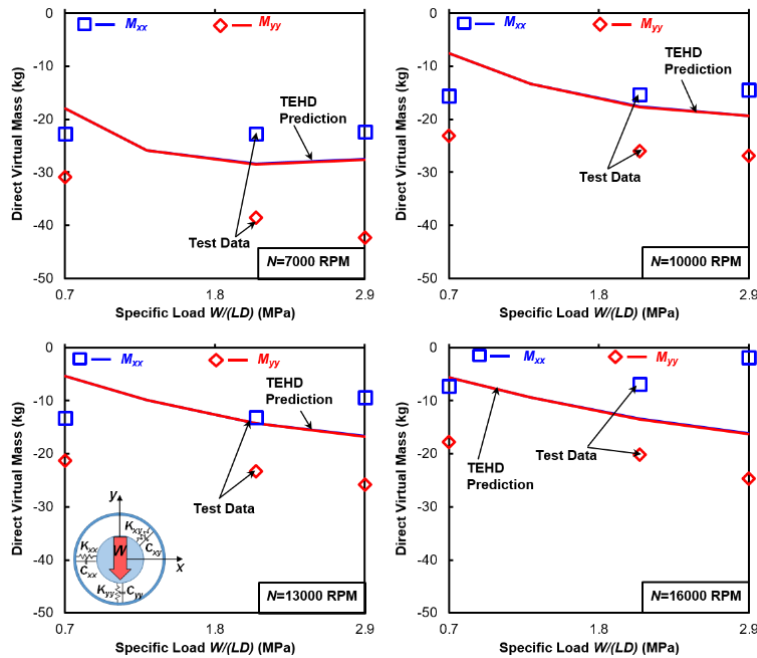

Figure 32: Direct virtual mass coefficients (M_{yy}, M_{xx}) versus specific load for operation at shaft speed 7 kRPM to 16 kRPM. TEHD prediction and test data in Ref. [4].

27

CONCLUSION

An accurate characterization of the static load performance in a bearing is paramount to also predict accurate rotordynamic force coefficients. An analysis that couples pressure generation to thermal effects in a bearing requires an accurate prediction of film and pad temperatures. Thus, this work introduces a simple yet effective thermal flow mixing model for the lubricant in a supply groove region that rectifies some limitations associated with a conventional hot oil carry over model (see Ref. [7]).

The conventional hot oil carry over model predicts a total flow rate of fresh (cold) lubricant that is supplied to a tilting pad journal bearing (TPJB) during operation, but it may differ with the actual flow. The novel mixing model utilizes a known total flow supply rate and allocates a portion of it to each feeding groove. For instance, Hagemann et al. [1] reduce the total flow rate supplied to a test TPJB by using axial end seals. For this case, a conventional hot oil carry over model over-estimates the total flow rate by over 70% which causes a 17 °C under prediction of pad surface temperature even with a large hot oil carry over factor ($\lambda = 0.9$). The novel thermal mixing model improves the accuracy of predicted pad surface temperatures by accounting for the recirculating lubricant in the grooves of a (flooded) bearing.

Furthermore, when a bearing housing is evacuated, considerable amounts of hot lubricant as well as freshly supplied oil discharge axially at the grooves between the pads [25]. The novel oil thermal mixing model takes into account the axially discharged (side leakage) flow, and utilizes an empirical coefficient (C_{gr}) to represent the efficiency of the bearing feeding arrangement. $0 < C_{gr} < 1$ specifies the contributions of hot upstream trailing edge flow and cold supply flow in a thermal energy exchange with discharge (side leakage) lubricant and the oil that churns in the groove.

Table 7 shows approximate ranges of the groove mixing efficiency parameter (C_{gr}) for various feeding arrangements and end seal configurations that deliver pad surface temperature prediction which best fit the test data in Refs. [1, 5]. As opposed to the hot oil carry over factor (λ), and since the known total supply flow is utilized, C_{gr} does not require modification for each operating condition. The predicted pad surface temperatures using the present thermal mixing model for the bearings in Refs. [1, 5] have less than 5 °C discrepancy with the test data for various operating conditions. Do note that the total oil supply flow rate is known at all instances.

Table 7: Recommended approximate range of groove efficiency parameter (C_{gr}) for various lubrication methods. Symbol ★ marks the C_{gr} magnitudes discussed in this lecture.
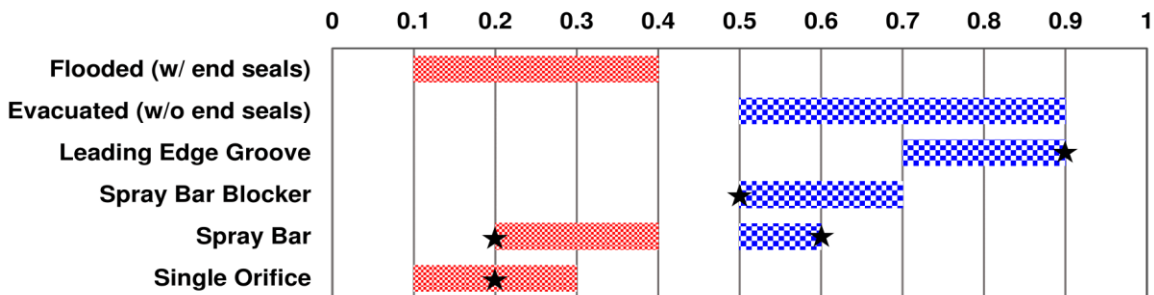
With respect to static load test data in Ref. [1], including thermally induced pad surface deformation improves the prediction of film thickness. The film thickness then generates a more accurate hydrodynamic pressure on each pad (about 20% improvement for peak film pressures). Accounting for pad thermoelastic deformations also reduces the predicted journal eccentricity in the load direction by ~25%, thus improving the correlation with test data.

As per the dynamic force coefficients, including pad thermoelastic deformations enhances the predictions, in particular it improves up to 28% the agreement of bearing direct stiffnesses with the test data in Ref. [5]. For a bearing operating at a high speed and under a low specific load, a pad thermally induced deformation is dominant since it reduces the bearing hot clearance and increases the predicted stiffness. As the applied static load increases, the pressure induced deformation becomes dominant and softens the bearing. Predicted bearing stiffnesses correlate well with the test data from Refs. [2, 4] with an average difference about 20%. Predictions for damping under estimate the test coefficients by about 40% which may be due to a large uncertainty in the used pivot stiffness.

The authors hope the novel thermal mixing model will find acceptance in the engineering community. There is still work to be done including more verifications against a wide variety of test data for bearings with various other geometries, number of pads, load orientations (LOP, LBP), lubrication delivery methods, and end-seal configurations. In this form, more accurate magnitudes for the

groove efficiency parameter (C_{gr}) applicable to a lubricant feeding and/or end seal arrangements can be quantified for ready engineering practice.

Acknowledgments

NOMENCLATURE

C_b , C_p	Bearing and pad radial clearances [m]
C_{xx} , C_{yy}	Bearing direct damping coefficients [N·s/m]
C_{gr}	Groove mixing coefficient [-]
C_i	demand parameter (C_i) for the ith groove [-]
c_p	Lubricant specific heat [J/kg °K]
e	Journal eccentricity [m]
D	Shaft diameter [m]
H_{xx}, H_{yy}	Complex dynamic stiffness [N/m]
K_{xx}, K_{yy}	Bearing direct stiffness coefficients [N/m]
L	Bearing pad axial length [m]
N	Journal rotational speed [RPM], $N = \Omega\pi/30$
n	Number of pads (=grooves)
M_{xx}, M_{yy}	Bearing virtual mass [kg]
m	Bearing preload [-], $m = 1 - C_b/C_p$
Q	Lubricant flow [LPM]
T	Fluid temperature [°C]
W	Static load [N]
Φ	Heat flow [W·m²]
a	Fraction of total supply flow allocated to each groove [-]
λ	Hot oil carry over factor in the conventional model [-]
ω	Excitation frequency (Hz)
Subscripts	
gr	Churning lubricant enclosed in the groove region
LE, TE	Leading edge and trailing edge of a pad
s	Shaft
$sump$	Region enclosed by back of a pad and housing
sup	Supply (fresh) lubricant
SL	Side leakage
Superscripts	
i	i^{th} pad (downstream of ith groove)
$i-1$	$(i-1)^{th}$ pad (upstream of ith groove)

REFERENCES

[1] Hagemann, T., Kukla, S., and Schwarze, H., 2013, "Measurement and Prediction of the Static Operating Conditions of a Large Turbine Tilting-Pad Bearing Under High Circumferential Speeds and Heavy Loads," ASME Paper No. GT2013-95004.

[2] Kukla, S., Hagemann, T., and Schwarze, H., 2013, "Measurement and Prediction of the Dynamic Characteristics of a Large Turbine Tilting-Pad Bearing Under High Circumferential Speeds," ASME Paper No. GT2013-95074.

[3] Coghlan, D. M., and Childs, D. W., 2017, "Characteristics of a Spherical Seat TPJB With Four Methods of Directed Lubrication: Part 1-Thermal and Static Performance," ASME. J. Eng. Gas Turbines Power. , **139**(12).

[4] Coghlan, D. M., and Childs, D. W., 2017, "Characteristics of a Spherical Seat TPJB With Four Methods of Directed Lubrication—Part II: Rotordynamic Performance," ASME. J. Eng. Gas Turbines Power., **139**(12).

[5] Coghlan, D. M., 2014, "Static, Rotordynamic, and Thermal Characteristics of a Four Pad Spherical-Seat Tilting Pad Journal Bearing with Four Methods of Directed Lubrication," M.S. Thesis, Texas A&M University, College Station, TX, USA.

[6] Ettles, C., 1967, "Paper 15: Solutions for Flow in a Bearing Groove," Proc. IMechE: Part 3L, **182**(14), pp. 120-131.

[7] Mitsui, J., Hori, Y., and Tanaka, M., 1983, "Thermohydrodynamic Analysis of Cooling Effect of Supply Oil in Circular Journal Bearing," ASME J. Lubr. Technol., **105**(3), pp. 414-420.

[8] Heshmat, H., and Pinkus, O., 1986, "Mixing Inlet Temperatures in Hydrodynamic Bearings," ASME J. Tribol., **108**(2), pp. 231-244.

[9] Ettles, C. M. M., 1980, "The Analysis and Performance of Pivoted Pad Journal Bearings Considering Thermal and Elastic Effects," ASME J. Lubr. Technol., **102**(2), pp. 182-191.

[10] Brito, F., Miranda, A., Claro, J. C. P., Teixeira, J., Costa, L., and Fillon, M., 2014, "Thermohydrodynamic Modelling of Journal Bearings Under Varying Load Angle and Negative Groove Flow Rate," Proc. IMechE Part J: Eng. Tribol., **228**(9), pp. 955-973.

[11] Brito, F., 2009, "Thermohydrodynamic Performance of Twin Groove Journal Bearings Considering Realistic Lubricant Supply Conditions: A Theoretical and Experimental Study," University of Minho, Braga, Portugal.

[12] Rindi, A., Rossin, S., Conti, R., Frilli, A., Galardi, E., Meli, E., Nocciolini, D., and Pugi, L., 2016, "Efficient Models of Three-Dimensional Tilting Pad Journal Bearings for the Study of the Interactions Between Rotor and Lubricant Supply Plant," ASME J. Comput. Nonlinear. Dyn., **11**(1), p. 011011.

[13] Suh, J., and Palazzolo, A., 2015, "Three-Dimensional Dynamic Model of TEHD Tilting-Pad Journal Bearing-Part II: Parametric Studies," ASME J. Tribol., **137**(4), p. 041704.

[14] He, M., Cloud, C. H., Byrne, J. M., and Vázquez, J. A., 2012, "Steady State Performance Prediction of Directly Lubricated Fluid Film Journal Bearings," Proceedings of the 41st Turbomachinery Symposium, The Turbomachinery Laboratory, Texas A&M University, September 24-27, Houston, Texas, USA.

[15] Nicholas, J. C., 2003, "Tilting Pad Journal Bearings With Spray-Bar Blockers and By-Pass Cooling for High Speed, High Load Applications," Proceedings of the 32nd Turbomachinery Symposium, The Turbomachinery Laboratory, Texas A&M University, September 21-24, Houston, Texas, USA, p. 27.

[16] Ettles, C., 1969, "Paper 11: Hot Oil Carry-Over in Thrust Bearings," Proc. IMechE: Part 3L, **184**(12), pp. 75-81.

[17] San Andrés, L., and Tao, Y., 2013, "The Role of Pivot Stiffness on the Dynamic Force Coefficients of Tilting Pad Journal Bearings," ASME J. Eng. Gas Turb. Pow., **135**(11), p. 112505.

[18] San Andrés, L., 2012, *Modern Lubrication Theory*," Thermohydrodynamic Bulk-Flow Model in Thin Film Lubrication", Notes 10, Texas A&M University Digital Libraries, http://oaktrust.library.tamu.edu/handle/1969.1/93197 [Accessed April 2017].

[19] Varela, A. C., Fillon, M., and Santos, I. F., 2012, "On the Simplifications for the Thermal Modeling of Tilting-Pad Journal Bearings Under Thermoelastohydrodynamic Regime," ASME Paper No. GT2012-68329, ASME Turbo Expo 2012: Turbine Technical Conference and Exposition, June 11-15, Copenhagen, Denmark, pp. 823-835.

[20] Abdollahi, B., 2017, "A Computational Model for Tilting Pad Journal Bearings: Accounting for Thermally Induced Pad Deformations and Improving a Feeding Groove Thermal Mixing Model," M.S. Thesis, Texas A&M University, College Station, TX, USA.

[21] Pinkus, O., 1990, Thermal Aspects of Fluid Film Tribology,, ASME Press, pp. 188-197.

[22] He, M., Allaire, P., Barrett, L., and Nicholas, J., 2005, "Thermohydrodynamic Modeling of Leading-Edge Groove Bearings Under Starvation Condition," Trib. Trans., **48**(3), pp. 362-369.

[23] San Andrés, L., 2012, *Modern Lubrication Theory*, " Derivation of the Classical Reynolds Equation for Thin Film Flows," Texas A&M University Digital Libraries, http://oaktrust.library.tamu.edu/handle/1969.1/93197 [Accessed April 2017].

[24] Ha, H. C., Kim, H. J., and Kim, K. W., 1995, "Inlet Pressure Effects on the Thermohydrodynamic Performance of a Large Tilting Pad Journal Bearing," ASME J. Tribol., **117**(1), pp. 160-165.

[25] Nicholas, J. C., Elliott, G., Shoup, T. P., and Martin, E., 2008, "Tilting Pad Journal Bearing Starvation Effects," Proceedings of the 37th Turbomachinery Symposium, The Turbomachinery Laboratory, Texas A&M University, September 15-18, Houston, Texas, USA, pp. 8-11.

[26] San Andrés, L., Koo, B., and Hemmi, M., 2017, "A Flow Starvation Model for Tilting Pad Journal Bearings and Evaluation of Frequency Response Functions: A Contribution Towards Understanding the Onset of Low Frequency Shaft Motions," ASME Paper No. GT2017-64822.

[27] He, M., 2003, "Thermoelastohydrodynamic Analysis of Fluid Film Journal Bearings," PhD Thesis, University of Virginia, Charlottesville, VA, USA.

[28] He, M., Allaire, P., Barrett, L., and Nicholas, J., 2002, "TEHD Modeling of Leading Edge Groove Tilting Pad Bearings," Proc. 6th International Conference on Rotor Dynamics (IFTOMM), Sydney, September.

[29] Harris, J. M., 2008, "Static Characteristics and Rotordynamic Coefficients of a Four-Pad Tilting-Pad Journal Bearing With Ball-in-Socket Pivots in Load-Between-Pad Configuration," M.S. Thesis, Texas A&M University, College Station, TX, USA.